Chinese Journal of Natural Medicines

Bisdemethoxycurcumin suppresses liver fibrosis-associated hepatocellular carcinoma *via* inhibiting CXCL12-induced macrophage polarization

Wei Yuan, Xinxin Zeng, Bin Chen, Sihan Yin, Jing Peng, Xiong Wang, Xingxing Yuan, Kewei Sun

Citation: Wei Yuan, Xinxin Zeng, Bin Chen, Sihan Yin, Jing Peng, Xiong Wang, Xingxing Yuan, Kewei Sun, Bisdemethoxycurcumin suppresses liver fibrosis-associated hepatocellular carcinoma *via* inhibiting CXCL12-induced macrophage polarization, Chinese Journal of Natural Medicines, 2025, 23(10), 1232-1247. doi: 10.1016/S1875-5364(25)60871-5.

View online: https://doi.org/10.1016/S1875-5364(25)60871-5

Chinese Journal of Natural Medicines 23 (2025) 1232-1247

Contents lists available at ScienceDirect

Chinese Journal of Natural Medicines

journal homepage: www.cjnmcpu.com/

Original article

Bisdemethoxycurcumin suppresses liver fibrosis-associated hepatocellular carcinoma *via* inhibiting CXCL12-induced macrophage polarization

Wei Yuan[a], Xinxin Zeng[c], Bin Chen[a], Sihan Yin[a], Jing Peng[a], Xiong Wang[a], Xingxing Yuan[b,*], Kewei Sun[a,*]

[a] *Department of Hepatology, First Affiliated Hospital of Hunan University of Chinese Medicine, Changsha 410000, China*
[b] *Department of Gastroenterology, Heilongjiang Academy of Traditional Chinese Medicine, Harbin 150001, China*
[c] *Department of Hepatobiliary Surgery, Hunan Provincial People's Hospital, The First Hospital of Hunan Normal University, Changsha 410005, China*

ARTICLE INFO

Article history:
Received 19 August 2024
Revised 3 November 2024
Accepted 7 November 2024
Available online 20 October 2025

Keywords:
Liver fibrosis-associated hepatocellular carcinom
Bisdemethoxycurcumin
CXCL12
β-Catenin/TCF4
M2 macrophage polarization

ABSTRACT

Chronic, unresolved inflammation correlates with persistent hepatic injury and fibrosis, ultimately progressing to hepatocellular carcinoma (HCC). Bisdemethoxycurcumin (BDMC) demonstrates therapeutic potential against HCC, yet its mechanism in preventing hepatic "inflammation-carcinoma transformation" remains incompletely understood. In the current research, clinical HCC specimens underwent analysis using hematoxylin-eosin (H&E) staining and immunohistochemistry (IHC) to evaluate the expression of fibrosis markers, M2 macrophage markers, and CXCL12. *In vitro*, transforming growth factor-β1 (TGF-β1)-induced LX-2 cells and a co-culture system of LX-2, THP-1, and HCC cells were established. Cell functions underwent assessment through 3-(4,5-dimethylthiazol-2-yl)-2,5-diphenyltetrazolium bromide (MTT), flow cytometry, and Transwell assays. Reverse transcription-quantitative polymerase chain reaction (RT-qPCR), Western blotting and immunofluorescence evaluated the differential expression of molecules. The interaction between *β*-catenin/TCF4 and CXCL12 was examined using co-immunoprecipitation (Co-IP), dual luciferase, and chromatin immunoprecipitation (ChIP) assays. A DEN-induced rat model was developed to investigate BDMC's role in liver fibrosis-associated HCC (LFAHCC) development *in vivo*. Our results showed that clinical HCC tissues exhibited elevated fibrosis and enriched M2 macrophages. BDMC delayed liver fibrosis progression to HCC *in vivo*. BDMC inhibited the inflammatory microenvironment induced by activated hepatic stellate cells (HSCs). Furthermore, BDMC suppressed M2 macrophage-induced fibrosis and HCC cell proliferation and metastasis. Mechanistically, BDMC repressed TCF4/*β*-catenin complex formation, thereby reducing CXCL12 transcription in LX-2 cells. Moreover, CXCL12 overexpression reversed BDMC's inhibitory effect on macrophage M2 polarization and its mediation of fibrosis, as well as HCC proliferation and metastasis. BDMC significantly suppressed LFAHCC development through CXCL12 in rats. In conclusion, BDMC inhibited LFAHCC progression by reducing M2 macrophage polarization through suppressing *β*-catenin/TCF4-mediated CXCL12 transcription.

1. Introduction

Hepatocellular carcinoma (HCC) ranks as the sixth most prevalent cancer globally and represents the third leading cause of cancer-related mortality [1]. According to the National Cancer Institute's SEER database, HCC patients in the United States (US) demonstrate a five-year survival rate of 19.6%, which decreases significantly to 2.5% in cases of metastatic HCC [2]. Research has established a strong correlation between chronic inflammation and tumorigenesis in human cancers [3]. HCC demonstrates a particular association with chronic inflammation and fibrosis, characterized as the hepatic inflammation-fibrosis-cancer axis [4]. Notably, 80 to 90% of HCC cases present with underlying cirrhosis stemming from chronic liver inflammation [5]. Furthermore, research confirms that hepatic stellate cells (HSCs) activation promotes progression from hepatic fibrosis to cirrhosis and subsequent tumorigenesis, thereby accelerating cancer development [6]. Zhang R *et al.* demonstrated that activated HSCs promote HCC cell malignancy through periostin secretion [7]. Consequently, understanding the role of activated HSCs in promoting hepatic "inflammation-fibrosis-carcinoma transformation" and its underlying mechanisms remains crucial.

The inflammatory microenvironment, modulated by macrophage polarization, serves as a critical factor in promoting fibrosis and tumor progression [8, 9]. Within the tumor environment, macrophages interact with tumor cells to influence tumorigenesis and metastasis [10, 11]. Macrophages typically manifest in two distinct phenotypes: M1-like and M2-like macrophages. M1 macrophages exhibit proinflammatory and anti-tumor characteristics, expressing tumor necrosis factor-α (TNF-α), interleukin (IL)-1β, IL-12, C-C motif chemokine ligand 2 (CCL2), inducible nitric oxide synthase (iNOS), and reactive oxygen species (ROS).

* Corresponding author.
E-mail addresses: jackie198711@163.com (X. Yuan); keweisun550@163.com (K. Sun)

https://doi.org/10.1016/S1875-5364(25)60871-5

Conversely, M2 macrophages display anti-inflammatory and protumorigenic properties, promoting fibrosis and tumor progression through the secretion of cytokines such as IL-10 and transforming growth factor-β1 (TGF-β1)[12]. This M2 phenotype polarization significantly influences liver fibrosis progression and subsequent HCC development [13, 14].

Our previous research demonstrated that miR-126 downregulation inhibited tumorigenesis in a murine colitis-associated colorectal cancer model by suppressing macrophage function and modifying the inflammatory environment *via* CXCL12 [15]. CXCL12 facilitates cell recruitment, migration, activation, and homing in liver diseases, with serum levels correlating to liver inflammation or fibrosis severity across various etiologies [16, 17]. Research indicates that activated HSCs promote M2 macrophage polarization through chemokine production [12]. This evidence suggests CXCL12's potential involvement in liver fibrosis-associated HCC (LFAHCC) progression. LX-2 cells, a human HSC line, provide an *in vitro* model for investigating HSCs activation and its impact on liver fibrosis and tumor progression. Upon activation, LX-2 cells generate fibrotic markers and chemokines, including CXCL12, contributing to macrophage polarization and the liver disease tumor microenvironment [18].

Bisdemethoxycurcumin (BDMC), a curcumin derivative, exhibits significant anti-tumor, anti-mutagenic, and anti-metastasis properties [19]. Notably, BDMC demonstrates ameliorating effects on various stages of hepatic "inflammation-fibrosis-carcinoma transformation". Evidence shows that BDMC alleviates hepatitis by reducing inflammatory responses through modulation of nuclear factor κB (NF-κB) and TGF-β signaling pathways [20]. Additionally, BDMC prevents hepatic fibrosis by inducing apoptosis in activated HSCs [21]. Furthermore, BDMC treatment inhibits HCC cell proliferation through protein kinase B (Akt) signaling inactivation [22]. However, the precise mechanism through which BDMC influences hepatic "inflammation-fibrosis-carcinoma transformation" requires further elucidation.

Wnt/*β*-catenin signaling activation plays a significant role in the progression of liver cancer associated with hepatitis C virus infection and liver fibrosis [23]. Akcora B O, *et al.* demonstrated that *β*-catenin/CBP inhibitor ICG-001 improved liver fibrosis *in vivo* by deactivating the canonical Wnt signaling pathway through suppression of stromal CXCL12 [24]. The Wnt/*β*-catenin signaling pathway exhibits frequent activation in HCC and maintains tumor initiation cells, drug resistance, tumor progression, and metastasis [25]. Research indicates that BDMC inactivates the Wnt/*β*-catenin pathway by reducing nuclear *β*-catenin expression [26]. Additionally, Wnt/*β*-catenin activation facilitates the formation of an inflammatory microenvironment during cancer tumorigenesis [27, 28]. Therefore, investigating BDMC's influence on the Wnt/*β*-catenin pathway and its therapeutic effects in liver fibrosis and HCC progression remains essential.

Canonical Wnts facilitate *β*-catenin stabilization and promote TCF4/*β*-catenin transcriptional complex formation [29]. Wnt ligands inhibit *β*-catenin degradation by preventing its phosphorylation by GSK-3β [30]. Nevertheless, the role of Wnt/*β*-catenin signaling as a target of BDMC in regulating hepatic "inflammation-fibrosis-carcinoma transformation" remains inadequately understood. Bioinformatics analysis revealed multiple TCF4 binding sites within the CXCL12 promoter region. This suggests that BDMC might regulate hepatic "inflammation-fibrosis-carcinoma transformation" through the Wnt/*β*-catenin signaling pathway by inhibiting CXCL12.

This study examines the hypothesis that liver fibrosis progression to HCC may be modulated through M2 macrophage polarization regulation and the Wnt/*β*-catenin signaling pathway. We suggest that BDMC may inhibit TCF4/*β*-catenin complex formation, thereby reducing CXCL12 transcription, a crucial factor in macrophage polarization and tumor progression.

2. Material and methods

2.1. Clinical sample collection

HCC tissues and adjacent normal tissues (n = 30) were obtained from the First Hospital of Hunan University of Chinese Medicine (Changsha, Hunan, China) and Hunan Provincial People's Hospital (Changsha, Hunan, China). The HCC sample selection criteria included: (1) HCC diagnosis confirmation through histopathological examination, (2) absence of prior chemotherapy or radiotherapy treatment, and (3) age > 18 years. Exclusion criteria comprised: (1) secondary liver tumors or other malignancies, (2) liver diseases unrelated to HCC, and (3) pregnancy. Clinical and pathological data collection proceeded with written informed consent. Each tissue sample underwent formalin fixation. The Ethics Committee of the First Hospital of Hunan University of Chinese Medicine (Changsha, China) approved the study.

2.2. Cell culture and treatment

HSCs (LX-2), HCC cell lines (HepG2 and Huh-7), and human monocytes (THP-1 cells) were obtained from American Type Culture Collection (ATCC, VA, USA). LX-2 and HCC cells were cultured in DMEM (Thermo Fisher Scientific, MA, USA) containing 10% FBS (Thermo Fisher Scientific), 1% penicillin, and 1% streptomycin. In addition, THP-1 cells were cultured in RPMI-1640 medium (Thermo Fisher Scientific) containing 10% fetal bovine serum (FBS, Thermo Fisher Scientific), 1% penicillin, and 1% streptomycin. All cells were cultured in condition with 5% CO_2 and 37 °C. To induce fibrosis *in vitro*, LX-2 cells were exposed to 5 ng·mL^{-1} TGF-β1 (Sigma-Aldrich, MO, USA) for 48 h. THP-1 cells were incubated with phorbol 12-myristate 13-acetate (PMA, 100 ng·mL^{-1}; Peprotech, MA, USA) for 48 h to induce macrophage formation. To clarify the role of BDMC, LX-2 cells were exposed to 30 μmol·L^{-1} BDMC (Sigma-Aldrich) for 24 h. To overexpress or block CXCL12, LX-2 cells were treated with 20 nmol·L^{-1} recombinant CXCL12 (Sigma-Aldrich) or 5 nmol·L^{-1} AMD3100 (Sigma-Aldrich) for 24 h.

2.3. Cell transfection

The complete complementary deoxyribonucleic acid (cDNA) encoding TCF4 or *β*-catenin was amplified by polymerase chain reaction (PCR) and subcloned into a modified pcDNA3.1 vector (Genepharma, Shanghai, China). LX-2 cells underwent transfection with the aforementioned plasmids or their corresponding controls using Lipofectamine 3000 (Invitrogen, CA, USA) following the manufacturer's protocol. After 48 h, cells were collected for subsequent analysis.

2.4. Cell co-culture

THP-1 cells were differentiated into macrophages using 150 nmol·L^{-1} PMA (Peprotech), followed by co-culture with differently treated LX-2 cells. Subsequently, THP-1 cells were harvested to evaluate the M1/M2 macrophage phenotype. These THP-1 cells were then collected and co-cultured with LX-2 cells or HCC cells. Co-cultured LX-2 cells were isolated for fibrosis investigation, while HCC cells were collected for migration and invasion assays.

2.5. 3-(4,5-Dimethylthiazol-2-yl)-2,5-diphenyltetrazolium bromide (MTT) assay

Cell viability after various treatments was assessed using an MTT kit (Beyotime, Shanghai, China). Cells were seeded into 96-

well plates at a density of 1 × 10^4 cells/well and cultured overnight. The cells were then incubated with 10 μL of MTT solution for 2 h. Subsequently, the supernatants were removed, and DMSO was added to each well. Absorbance measurements were taken at 490 nm.

2.6. Cell apoptosis detection

LX-2 cells (2 × 10^6) were centrifuged and resuspended in 500 μL of 1 × Annexin-binding buffer (BD, NJ, USA). Cells underwent treatment with 5 μL Annexin V-FITC (BD) and propidium iodide (PI, BD) for 15 min. Apoptosis analysis was performed using a flow cytometer (BD).

2.7. Western blotting

Nucleocytoplasmic separation was performed using the nuclear and cytoplasmic extraction kit (Beyotime). Treated cells were centrifuged at 500 g for 3 min after washing with cold phosphate-buffered saline (PBS). The cell pellet was incubated with ice-cold cytosol extraction buffer on ice for 1 min, followed by centrifugation at 12 000 *g* for 5 min at 4 °C. The supernatant containing cytoplasmic components was collected, and the insoluble nuclear fraction was resuspended. Proteins were extracted using RIPA lysis buffer (Beyotime) and quantified using a BCA kit (Beyotime). The proteins were separated by 10% SDS-PAGE (30 μg/lane) and transferred onto PVDF membranes. The membranes were incubated with primary antibodies at 4 °C overnight. The antibodies used were: anti-*α*-SMA (ab124964, 1∶5000, antibody (Abcam), Shanghai, China), anti-TCF4 (ab217668, 1:10000, Abcam), anti-*β*-catenin (ab32572, 1∶5000, Abcam), anti-E-cadherin (ab40772, 1∶1000, Abcam), anti-*N*-cadherin (ab76011, 1∶5000, Abcam), anti-CXCL12 (ab155090, 1∶10000, Abcam), anti-fibronectin (ab2413, 1∶1000, Abcam), anti-collagen I (ab138492, 1∶1000, Abcam), Lamin B1 (ab16048, 1:1000, Abcam) and anti-GAPDH (ab8245, 1∶10000, Abcam). Subsequently, the membranes were incubated with secondary antibodies (horse radish peroxidase (HRP)-conjugated, ab288151 and ab6789, 1∶5000, Abcam) at room temperature for 1 h. Protein bands were visualized using the ECL kit (Beyotime).

2.8. Immunofluorescence

Cells were fixed with methanol and permeabilized. The cells were incubated overnight at 4 °C with anti-CD206 (ab64693, 1∶100, Abcam) or anti-CD86 (ab239075, 1∶100, Abcam). Subsequently, cells were incubated with the corresponding secondary Abcam in darkness for 1 h. The cells were then examined under a fluorescence microscope (Olympus, Tokyo, Japan).

2.9. Reverse transcription-quantitative PCR (RT-qPCR)

Total ribonucleic acid (RNA) extraction was performed using TRIzol® reagent (Invitrogen). cDNA synthesis was conducted using the iScript cDNA Synthesis kit (Bio-Rad, CA, USA) and analyzed through RT-qPCR using SYBR Green (ELK, CO, USA). The protocol consisted of: 94 °C for 2 min, followed by 40 cycles (94 °C for 30 s and 45 s at 55 °C). The primer sequences are presented in Supplementary Table 1.

2.10. Dual luciferase assay

The sequences (site1: CGCCACCTGCCCG; site2: TCCAGCTGCC) of the CXCL12 promoter containing TCF4 and *β*-catenin binding sites were incorporated into the pGL3 vector. LX-2 cells underwent co-transfection with the constructed luciferase reporter vector and pcDNA3.1-control (NC) or TCF4 and *β*-catenin. Data analysis was performed using the Dual-Glo Luciferase Assay System (Promega, Shanghai, China) after 48 h of transfection.

2.11. Transwell assay

HCC cell migration and invasion were evaluated using a Transwell system (24-wells, 8 μm pore size with poly-carbonate membrane; BD). Cells underwent trypsinization and were seeded in the upper chamber with serum-free media at a density of 1 × 10^5 cells/chamber. The lower chamber contained 800 μL medium with 10% FBS as a chemoattractant. After 48 h, cells on the lower filter side were fixed in 3.8% formaldehyde for 20 min and stained with 0.1% crystal violet solution. For invasion assessment, the upper chamber received a coating of extracellular matrix (BD), a soluble basement membrane matrix. The remaining procedure followed the migration assay protocol.

2.12. Co-Immunoprecipitation (Co-IP) assay

LX-2 cells underwent lysis in IP lysis buffer, and the cell lysates were incubated with primary antibody (anti-TCF4, #2569, Cell Signaling Technology, MA, USA) or negative control IgG at 4 °C for 2 h, followed by protein-A/G agarose treatment overnight at 4 °C. The complex was rinsed and boiled after bead mixing. Western blotting was subsequently employed for sample examination.

2.13. Chromatin immunoprecipitation (ChIP) assay

LX-2 cells were cross-linked using 1% formaldehyde for 10 min at room temperature, with the reaction terminated by glycine for 5 min. The cell pellet underwent resuspension in lysis buffer, and DNA was fragmented into 100–300 bp segments through sonication. The samples were incubated with TCF4 antibody (anti-TCF4, ab217668, Abcam), *β*-catenin antibody (anti-*β*-catenin, ab32572, Abcam), or control IgG antibody overnight, followed by protein-A/G agarose bead incubation for 2 h at 4 °C. The binding complexes underwent Proteinase K digestion after washing. Precipitated DNA was analyzed using RT-qPCR.

2.14. In vivo experiments

Hepatic "inflammation-fibrosis-carcinoma transformation" was induced using DEN treatment as previously described [4]. SD rats (*n* = 150; aged 6–8 weeks) were obtained from Hunan SJA Laboratory Animal Co., Ltd. (Hunan, China). The ethical committee of the First Hospital of Hunan University of Chinese Medicine (Changsha, Hunan, China) approved this study. After one week of acclimatization, rats were randomly assigned to control, DEN, DEN + DMSO, DEN + BDMC, DEN + CXCL12 and DEN + BDMC + CXCL12 groups (*n* = 25 each). The control group received intraperitoneal saline solution (0.9%) twice weekly. The DEN group received 30 mg·kg^{-1} DEN (Sigma-Aldrich) twice weekly for 11 weeks. Following the 11-week DEN administration, DEN was discontinued, and the animals were monitored until 20 weeks. Concurrently, rats in DEN + BDMC and DEN + BDMC + CXCL12 groups received 25 mg·kg^{-1} BDMC intraperitoneally administered every other day after 4 weeks of DEN administration as previously reported [31]. Additionally, rats in DEN + CXCL12 and DEN + BDMC + CXCL12 groups received recombinant rat CXCL12 at 4 μg·kg^{-1}·d^{-1}. At 0, 6, 12 and 20 weeks, serum was collected for biochemical analysis (alanine aminotransferase (ALT), aspartate transaminase (AST), hyaluronidase (HA), laminin (LN), precollagen III *N*-terminal peptide (p-III-NP), IV collagenase (IV-C), IL-10, Arg-1 and TGF-β1) and liver tissues were collected for histological (hematoxylin-eosin (H&E) and Masson) and immunohistochemistry (IHC) detection (*α*-SMA, collagen I, CXCL12, and

CD206). The liver/body weight ratio was measured. Liver tissues were sectioned and fixed in 10% formalin for histopathology and immunohistochemical examinations. The remaining portions were frozen and stored at −80 °C until analysis. All experiments were conducted in accordance with NIH guidelines and received approval from the Animal Ethics Committee of the First Hospital of Hunan University ofChinese Medicine (Ethical code: EYFY20231113-110).

2.15. Enzyme linked immunosorbent assay (ELISA)

Serum levels of IV-C (E-EL-R3009, Eelabscience, Wuhan, China), AST (ab263883, Abcam), ALT (ab234579, Abcam), HA (ab304945, Abcam), LN (ab119573, Abcam), and p-III-NP (E-EL-R3024, Eelabscience) were measured using the corresponding ELISA kits following the manufacturer's protocols.

2.16. Morphometric evaluation

Hepatic tissues from experimental groups of rats were examined morphologically for visible neoplastic nodules at the time of sacrifice at the study's conclusion, as previously reported [32].

2.17. H&E and Masson staining

Tissues were fixed in formaldehyde neutral buffer and embedded in paraffin blocks. The sections (4 μm-thick) were stained with collagen-specific Masson's trichrome for fibrosis detection or with H&E for cell morphometry. The Ishak scoring system was applied to grade hepatic fibrosis: grade 0, no fibrosis; grade 1, slight fibrous expansion of portal areas; grade 2, serious fibrous expansion; grade 3, serious fibrous expansion with occasional portal-to-portal bridging; grade 4, fibrous expansion of portal areas with marked portal to portal and/or portal to central bridging; grade 5, marked portal to portal and/or portal to central bridging with occasional nodules; grade 6, cirrhosis [33].

2.18. IHC staining

Tissue sections (4 μm thickness) were fixed and processed. Following deparaffinization and rehydration, antigen retrieval was performed using microwave treatment with sodium citrate buffer. Subsequently, samples underwent PBS washing for 5 min. The samples were then incubated in 3% H_2O_2 for 25 min, followed by washing and serum incubation for 30 min. Overnight incubation was performed with primary antibodies: anti-collagen I (ab279711 1∶500, Abcam), anti-CXCL12 (ab25117 or ab9797, 1∶500, Abcam), anti-α-SMA (ab124964, 1∶1000, Abcam), anti-CD206 (ab64693, 1∶100, Abcam), CD86 (ab220188, 1∶200, Abcam), Arg-1 (ab315110, 1∶5000, Abcam), IL-10 (ab34843, 1∶1000, Abcam) and TGF-β1 (ab215715, 1∶500, Abcam). The samples were then incubated with secondary antibody (HRP-labeled; 1∶200, Abcam) at 37 °C for 30 min. The tissues were subsequently incubated with diaminobenzidine (DAB) and analyzed under microscopic examination. The proportion of positively-stained cells was determined by counting 500 cells at 100 × magnification as previously described [34].

2.19. Statistical analysis

Each experiment was conducted with a minimum of three repetitions. Data are expressed as mean ± standard deviation. Statistical analyses were performed using GraphPad Prism 8.0 software. Differences between two groups were analyzed using unpaired student's *t*-test. For multiple group comparisons, one-way analysis of variance followed by Tukey's post hoc tests was employed. Statistical significance was established at P values < 0.05.

3. Results

3.1. HSCs-mediated liver fibrosis and macrophage M2 polarization were associated with HCC

Previous research indicates that HSCs-mediated liver fibrosis and macrophage polarization play crucial roles in LFAHCC progression [12, 35]. Histological changes in HCC were evaluated using H&E and IHC staining. Fig. 1A demonstrates that HCC tissues displayed disrupted liver tissue architecture, significant tumor cell infiltration, and fibrosis. Analysis of macrophage polarization and fibrosis indicators in HCC and adjacent normal tissues revealed significantly elevated levels of α-SMA (a fibrosis marker) in HCC tissues compared to adjacent normal tissues (Fig. 1B). Additionally, HCC tissues showed decreased expression of the M1-type marker CD86 and increased expression of the M2-type marker CD206 (Figs. 1C and 1D). The protein levels of M2 macrophage-secreted cytokines, including Arg-1, IL-10, and TGF-β1, were markedly elevated in HCC tissues relative to adjacent normal tissues (Figs. 1E–1G). CXCL12 is a chemokine associated with liver inflammation and fibrosis severity across various etiologies [17], and known to be produced by HSCs to induce M2 polarization of macrophages [12], showed significantly higher levels in HCC tissues compared to adjacent normal tissues (Fig. 1H). These findings demonstrate that HSCs-mediated liver fibrosis and macrophage M2 polarization correlate with HCC progression.

3.2. BDMC alleviated the progression of liver fibrosis to HCC

To investigate the biological role of BDMC in the transition from liver fibrosis to HCC, an animal study was conducted (Fig. 2A). Serum biochemical analyses were performed to evaluate hepatic function and fibrosis severity. As shown in Figs. 2B and 2C, serum levels of ALT, AST, HA, LN, P-III-NP, and IV-C increased significantly in the DEN-treated group, while BDMC administration prevented these elevations from the inflammation stage (week 6) through the fibrosis stage (week 12) to the HCC stage (week 20). DEN significantly elevated the liver/body weight ratio, whereas BDMC partially reversed this change at week 20 (Fig. 2D). Furthermore, pro-inflammatory factors such as IL-6, IL-1β, and TNF-α (M1-type markers) were dynamically upregulated in the model group during inflammation and liver fibrosis, while these changes were partially inhibited by pre-administration of BDMC at week 6 and week 12 (Fig. 2E). Serum levels of IL-10, Arg-1, and TGF-β1 (M2-type markers) gradually increased in the HCC stages in the model group compared to the control group from week 6 to week 20. The BDMC-treated group exhibited decreased levels of these markers compared to the model group (Fig. 2F). The increase in M2-type markers induced by DEN was more pronounced and sustained than that of M1-type markers, suggesting that the increase in M1-type markers might represent a transient response caused by compensatory stress in rats. The histopathological changes in the livers of different groups at different stages were shown in Figs. 2G–2H. Livers from the control group displayed normal histology, while DEN treatment resulted in progressive lesions, evolving from inflammation (6^{th} week), fibrosis (12^{th} week), to HCC (20^{th} week). At 6 weeks post-DEN injection (inflammation stage), chronic inflammatory infiltrates with diffuse ballooning degeneration, dilated lymph vessels, and proliferating bile ducts were observed in the portal area. Liver from rats pretreated with BDMC showed minimal hepatic injury, with only slight vascular congestion and focal lymphoplasmacytic infiltrates. After 12 weeks of DEN injury (fibrosis stage), the liver lobules in the model group showed disordered hepatocyte arrangement and extensive fibrous tissue deposition. Lipid droplets, hydropic degeneration, necrosis, and hepatocyte regen-

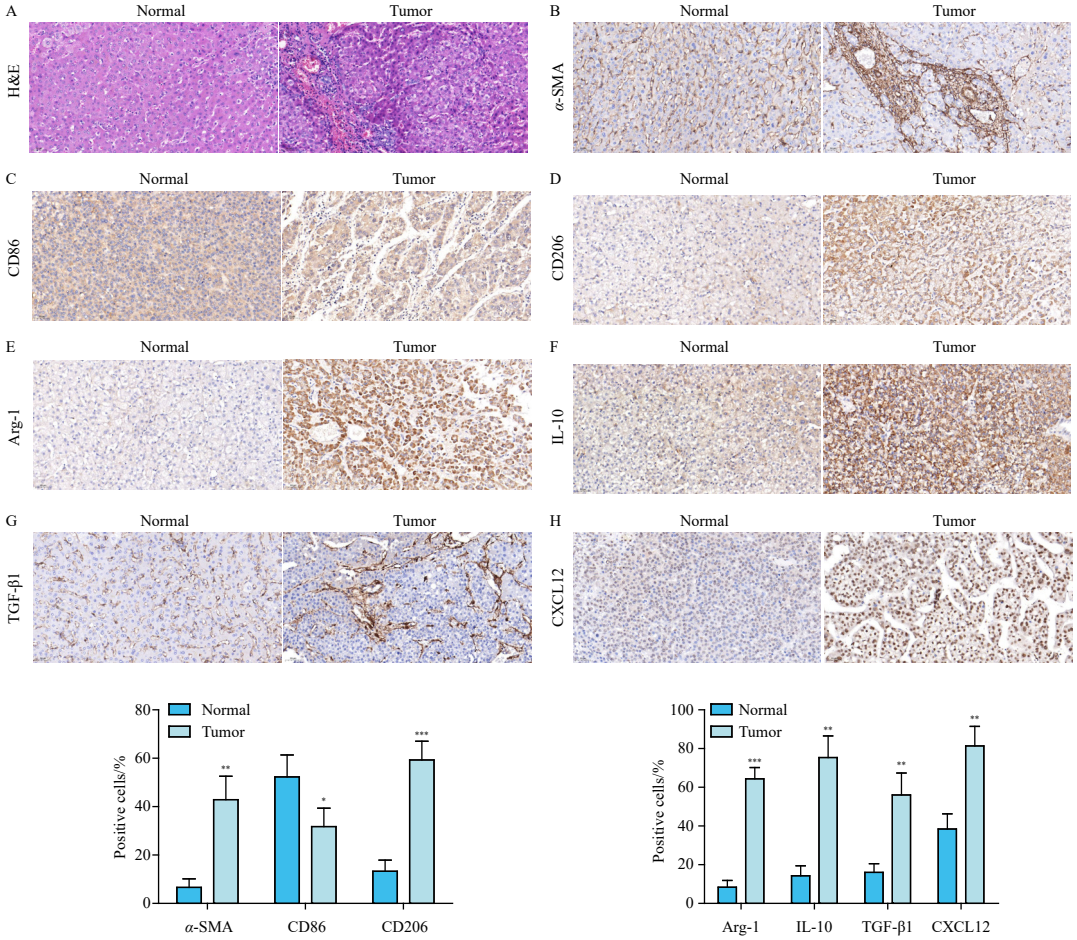

Fig. 1 Fibrosis and M2 macrophages were enriched in HCC tissues. (A) The histological changes of HCC tissues were observed by H&E staining. (B–H) The levels of α-SMA, CD86, CD206, Arg-1, IL-10, TGF-β1 and CXCL12 were detected in HCC tissues by IHC staining. Data were expressed as mean ± SD (n = 30). $^{*}P < 0.05$, $^{**}P < 0.01$, $^{***}P < 0.001$ *vs* Norma; Original magnification: 200 × .

eration were evident. BDMC pre-administration reduced the extent of DEN-induced liver fibrosis. After 20 weeks of DEN injection (HCC stage), the model group exhibited architectural loss, hepatic parenchyma with granular cytoplasm, and cancerous focus with patchy necrosis. Liver nodules contained relatively large hepatocytes with enlarged nuclei and eosinophilic cytoplasm surrounded by fibrotic stroma. DEN-bearing BDMC-treated groups showed moderate malignancy with focal necrosis and reduced mitotic count. Morphological changes were observed in the livers of different groups at week 20. As shown in Fig. 2I, control group livers appeared normal, brown, smooth and soft in texture, while DEN group livers were rough and nodular, with multiple white nodules, indicating HCC development. Pretreatment with BDMC significantly improved the recovery from DEN-induced liver structural damage. Lung metastasis nodules increased significantly after DEN treatment, while these pathological changes were ameliorated by BDMC treatment (Fig. 2J). Collectively, BDMC demonstrated the ability to alleviate the progression of liver fibrosis to HCC.

3.3. BDMC reduced M2 polarization induced by activated HSCs

To examine the effects of BDMC on LX-2 cells, TGF-β1 was utilized to induce HSC activation and fibrosis in LX-2 cells. The cells were subsequently treated with varying concentrations of BDMC. As shown in Figs. 3A and 3B, both BDMC and TGF-β1 had limited effects on LX-2 cell viability. TGF-β1 at concentrations of 5 and 10 ng·mL^{-1} significantly enhanced the expression of pro-fibrotic molecules, including α-SMA, collagen I and fibronectin, in LX-2 cells (Fig. 3C). BDMC at concentrations of 30 and 50 μmol·L^{-1} significantly suppressed the TGF-β1-induced elevation in these pro-fibrotic molecules (Fig. 3D). These results led to the selection of 5 ng·mL^{-1} of TGF-β1 and 30 μmol·L^{-1} of BDMC for subsequent experiments. Furthermore, while TGF-β1 stimulation decreased LX-2 cell apoptosis, BDMC treatment partially reversed this effect (Fig. 3E). LX-2 cells were co-cultured with PMA-differentiated THP-1 cells, after which THP-1 cells were collected for further analysis (Fig. 3F). A two-step co-culture system of macrophages and HSCs was established (Fig. 3F) to investigate BDMC's effect on macrophages. In this system, macrophages were first removed from the initial co-culture, where PMA-differentiated THP-1 cells in the upper chamber were co-cultured with LX-2 cells in the lower chamber for 2 days. These 'educated' macrophages were subsequently transferred to a second co-culture system with untreated HCC cell lines (HepG2 and Huh-7) for an additional 2 days. The findings demonstrated that activated LX-2 cells significantly decreased CD86 (M1-type markers) expression while increasing CD206 (M2-type markers) expression in co-cultured macrophages, effects that were neutralized by BDMC (Fig. 3G). Additionally, macrophages co-cultured with activated LX-2 cells showed significantly reduced levels of IL-6 and IL-1β (M1-type markers), while IL-10 and Arg-1 (M2-type markers) expressions were significantly increased; BDMC partially reversed these effects (Fig. 3H). These results indicate that BDMC reduced M2 polarization induced by activated HSCs.

3.4. BDMC inhibited liver fibrosis and HCC induced by M2-like macrophages

To evaluate the impact of BDMC on liver fibrosis and HCC de-

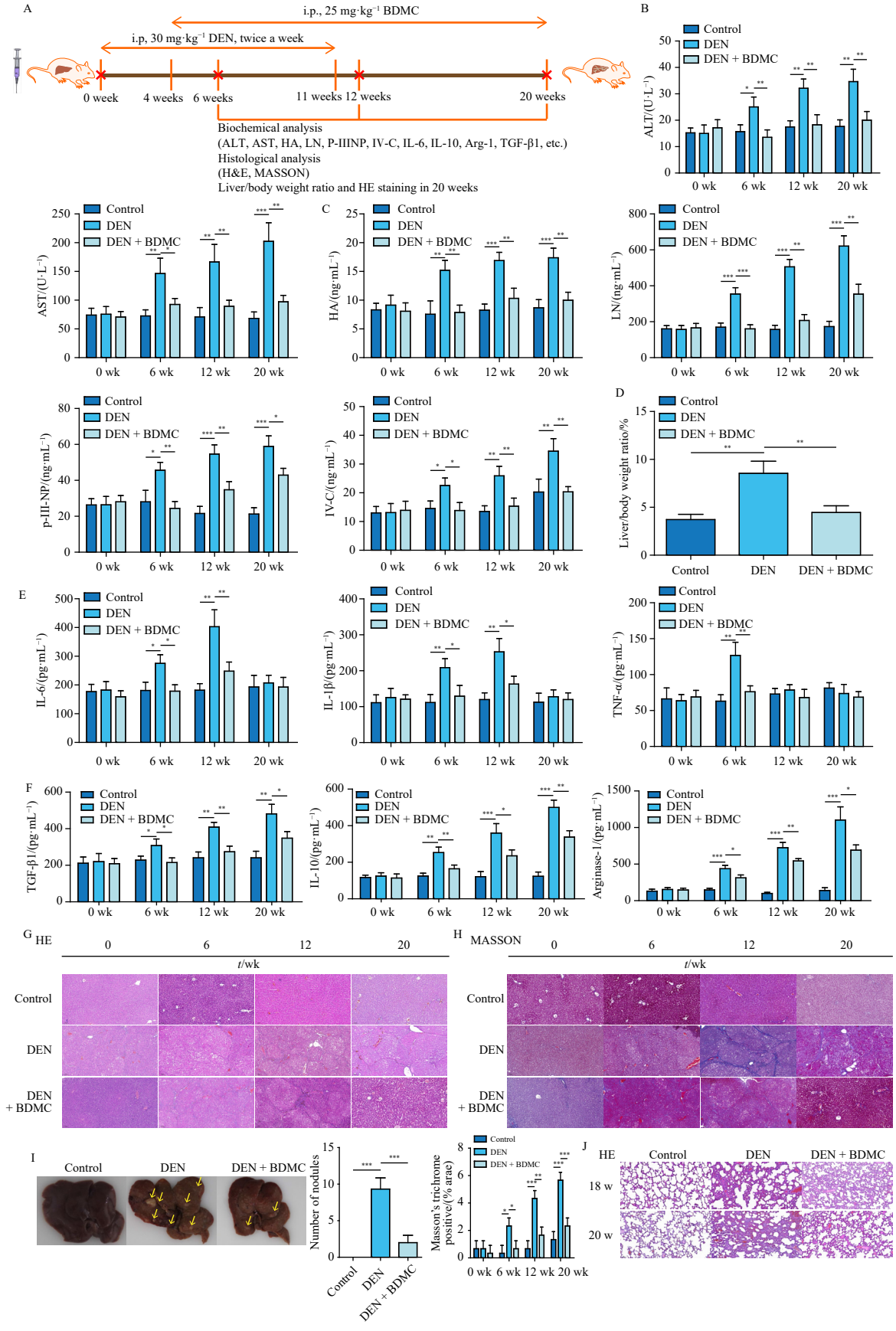

Fig. 2 BDMC alleviated the progression of liver fibrosis to HCC. (A) Animal experiments and sampling flowchart was presented. The DEN group was administered DEN at 30 mg·kg^{-1} twice a week for 11 weeks. BDMC was administered at a dose of 25 mg·kg^{-1} intraperitoneally every other day starting at week 4. (B–C) The contents of AST, ALT, HA, LN, P-III-NP and IV-C in serum of rats were tested by ELISA kits. (D) The liver/body weight ratio was calculated. (E) The concentrations of IL-1β, IL-6 and TNF-α in rat serum were detected by ELISA kits. (F) The concentrations of TGF-β1, IL-10 and Arg-1 in rat serum were detected by ELISA kits. (G–H) H&E and Masson staining results of rat liver tissues. (I) The images of liver tissue were presented. (J) H&E staining results of rat lung tissues. Data were expressed as mean ± SD (n = 6). $^{*}P < 0.05$, $^{**}P < 0.01$, $^{***}P < 0.001$. Original magnification: 100 × .

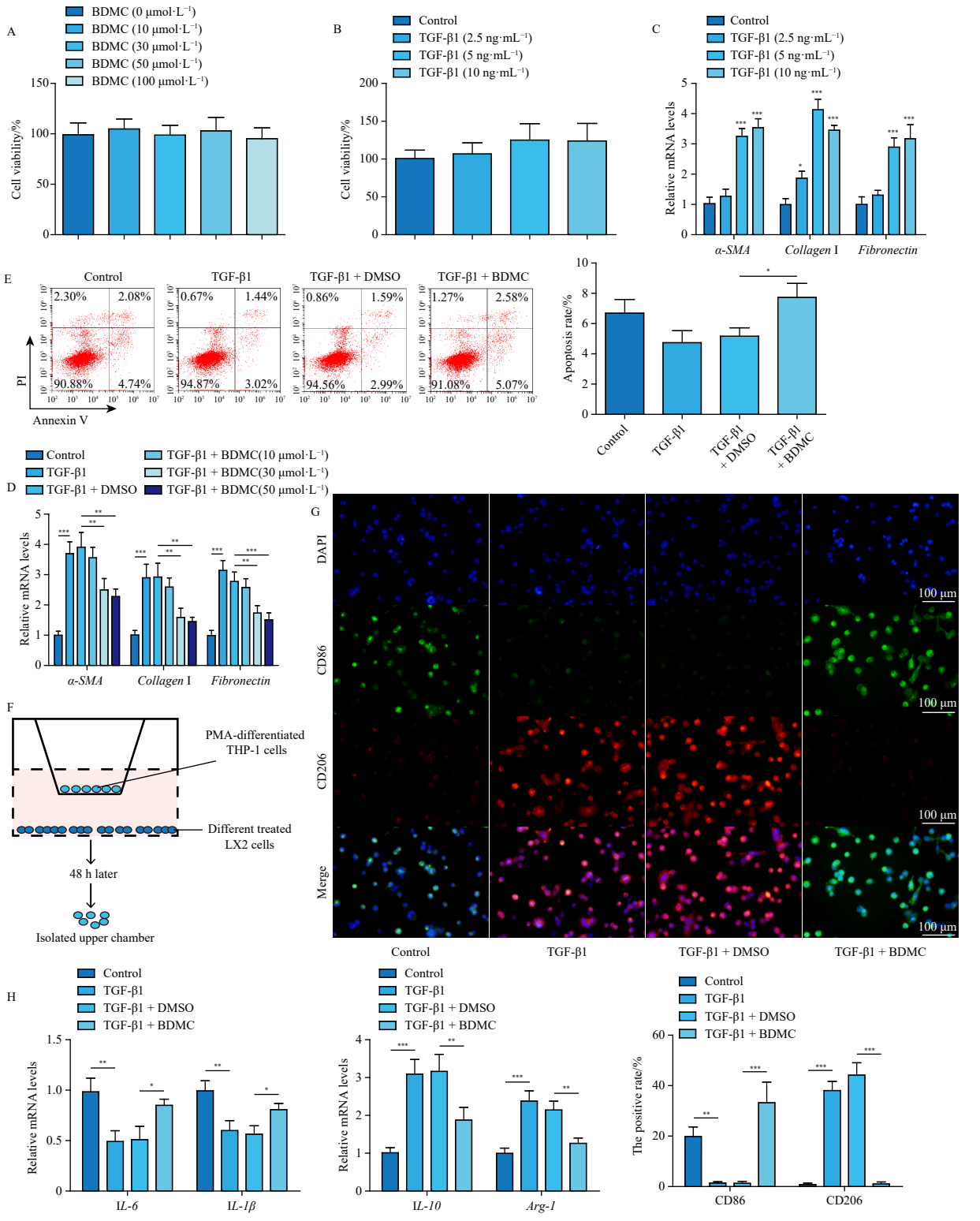

Fig. 3 BDMC reduced M2 polarization of macrophages induced by activated HSCs. (A) The viability was tested by MTT assay in LX-2 cells treated with 10, 30, 50 or 100 μmol·L^{-1} BDMC. (B) The viability was tested by MTT assay in LX-2 cells treated with 2.5, 5 or 10 ng·mL^{-1} TGF-β1. (C) The mRNA levels of *α-SMA*, *fibronectin* and *collagen I* were determined by RT-qPCR in LX-2 cells treated with 2.5, 5 or 10 ng·mL^{-1} TGF-β1. (D) The mRNA levels of *α-SMA*, *fibronectin* and *collagen I* were determined by RT-qPCR in LX-2 cells treated with TGF-β1, TGF-β1 + BDMC (10, 30, 50 μmol·L^{-1}). Cells were exposed to TGF-β1, TGF-β1 + DMSO or TGF-β1 + BDMC. (E) The apoptosis was examined by flow cytometry in LX-2 cells exposed to TGF-β1, TGF-β1 + DMSO or TGF-β1 + BDMC. Cells were exposed to TGF-β1, TGF-β1 + DMSO or TGF-β1 + BDMC, and then co-cultured with THP-1 cells for 48 h. Then, THP-1 cells were collected. (F) Co-culture schematic diagram. (G) The expression of CD86 and CD206 in co-cultured THP-1 cells were investigated by immunofluorescence staining. (H) The levels of IL-6, IL-1β, IL-10 and Arg-1 in co-cultured THP-1 cells were examined by RT-qPCR. Data were expressed as mean ± SD. All data were obtained from three independent experiments. $^{*}P < 0.05$, $^{**}P < 0.01$, $^{***}P < 0.001$.

velopment, PMA-differentiated THP-1 cells were co-cultured with LX-2 cells under various treatment conditions, followed by co-culture with HCC cells (HepG2 and Huh-7). LX-2 cells and HCC cells were subsequently collected for analysis (Figs. 4A and 4E). The results indicated that macrophages exhibited no significant influence on LX-2 cell activity (Fig. 4B). Furthermore, TGF-β1 significantly increased fibrotic messenger RNA (mRNA) and protein levels (collagen I, α-SMA and fibronectin) in LX-2 cells, an effect

partially reversed by BDMC treatment (Figs. 4C–4D). Additionally, PMA-differentiated THP-1 cells co-cultured with TGF-β1-induced LX-2 cells enhanced HCC cell viability and proliferation, which was partially suppressed by BDMC (Figs. 4F–4G). Moreover, PMA-differentiated THP-1 cells co-cultured with TGF-β1-induced LX-2 cells promoted HCC cell invasion and migration

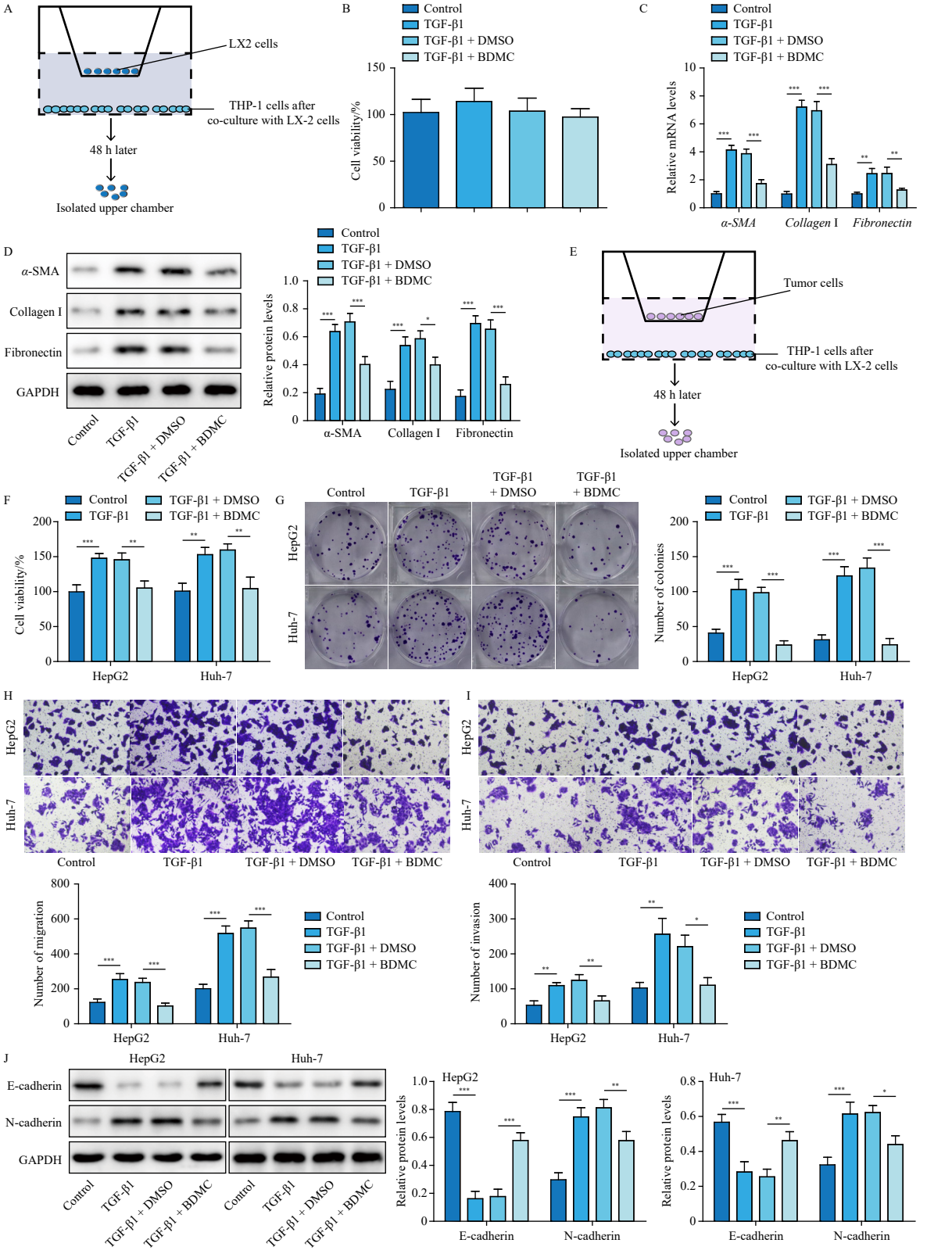

Fig. 4 BDMC inhibited liver fibrosis and HCC cells function induced by M2-like macrophages. PMA-induced THP-1 cells were harvested after co-cultured with LX-2 cells from above as M2-like macrophages. Then M2-like macrophages were co-cultured with LX-2 cells and HCC cells, respectively, and then LX-2 cells and HCC cells were collected for further analysis. (A) The schematic diagram of M2-like macrophages and LX-2 cells. (B) Cell viability of LX-2 cells was assessed by MTT assay. (C&D) Fibronectin, collagen I and α-SMA levels in co-cultured LX-2 cells were investigated by RT-qPCR and western blot. GAPDH was used for normalization. (E) The schematic diagram of M2-like macrophages and HCC cells. (F) The viability of co-cultured Huh-7 and HepG2 cells was tested by MTT assay. (G) The proliferation of co-cultured HCC cells was assessed by colony formation assay. (H&I) The migration and invasion of HCC cells were examined by transwell assay. (J) E-cadherin and N-cadherin levels in co-cultured HCC cells were tested by western blot. Data were expressed as mean ± SD. All data were obtained from three independent experiments. $^{*}P < 0.05$, $^{**}P < 0.01$, $^{***}P < 0.001$.

through E-cadherin downregulation and *N*-cadherin upregulation, effects substantially mitigated by BDMC (Figs. 4H–4J). These findings demonstrate that BDMC attenuated liver fibrosis and M2-like macrophages-mediated HCC.

3.5. BDMC prevented the formation of β-catenin/TCF4 complex

The Wnt/*β*-catenin signaling pathway demonstrates activation in HCC and serves a critical function in the progression of HCC associated with liver fibrosis [25]. As shown in Fig. 5A, TGF-β1 elevated TCF4 and *β*-catenin levels in LX-2 cells, an effect neutralized by BDMC treatment. Previous research has demonstrated that curcumin positively influences cancer prevention and tumor therapy through regulation of the Wnt/*β*-catenin pathway [36]. The present study revealed that TGF-β1 induced elevated levels of TCF4 and *β*-catenin in the nucleus of LX-2 cells, which was markedly reduced by BDMC (Fig. 5B). Furthermore, TGF-β1 substantially increased *β*-catenin/TCF4 complex expression, which was normalized by BDMC (Fig. 5C). These results indicate that BDMC prevented *β*-catenin/TCF4 complex formation in TGF-β1-induced HSC cells.

3.6. BDMC inhibited CXCL12 transcription via suppressing β-catenin/TCF4

A bioinformatics analysis revealed potential binding sites (site1 and site2, Fig. 6A) between TCF4 and the CXCL12 promoter region. Following TCF4/*β*-catenin overexpression in LX-2 cells, a significant elevation in TCF4/*β*-catenin levels was observed (Fig. 6B). Furthermore, overexpression of either TCF4 or *β*-catenin substantially increased CXCL12 levels in LX-2 cells (Fig. 6C). The overexpression of TCF4 or *β*-catenin significantly enhanced the luciferase activity of the CXCL12 promoter (Fig. 6D), while TCF4 and *β*-catenin antibodies successfully enriched the CXCL12 promoter region in LX-2 cells (Fig. 6E), demonstrating direct binding between TCF4/*β*-catenin and the CXCL12 promoter. Additionally, BDMC significantly reduced TGF-β1-induced elevation of CXCL12 levels in LX-2 cells, though this effect was notably reversed by TCF4 or *β*-catenin overexpression (Figs. 6F and 6G). These findings indicate that BDMC reduced CXCL12 transcription *via* suppression of *β*-catenin/TCF4.

3.7. CXCL12 reversed BDMC's inhibition of M2 polarization caused by activated HSCs

Previous research has established CXCL12 as a chemokine that attracts macrophages through CXCR4 binding. To examine the interaction between BDMC and CXCL12 in activated HSCs-mediated macrophage polarization, recombinant CXCL12 was administered to LX-2 cells. The results demonstrated that BDMC reduced CXCL12 levels in TGF-β1-treated LX-2 cells, with this effect significantly reversed by recombinant CXCL12 and enhanced by AMD3100 (CXCL12 inhibitor) (Fig. 7A). Cell viability studies revealed that while BDMC did not affect LX-2 cell viability, CXCL12 significantly enhanced it, and AMD3100 reduced it (Fig. 7B). Additionally, BDMC enhanced LX-2 cell apoptosis, but this effect was counteracted by recombinant CXCL12 and amplified by AMD3100 (Fig. 7C). Furthermore, recombinant CXCL12 reversed BDMC's stimulatory effect on M1-type markers and its inhibitory effect on M2-type markers, while AMD3100 demonstrated opposing effects (Figs. 7D–7E). These findings indicate that BDMC inhibited M2 polarization caused by activated HSCs *via* CXCL12 suppression.

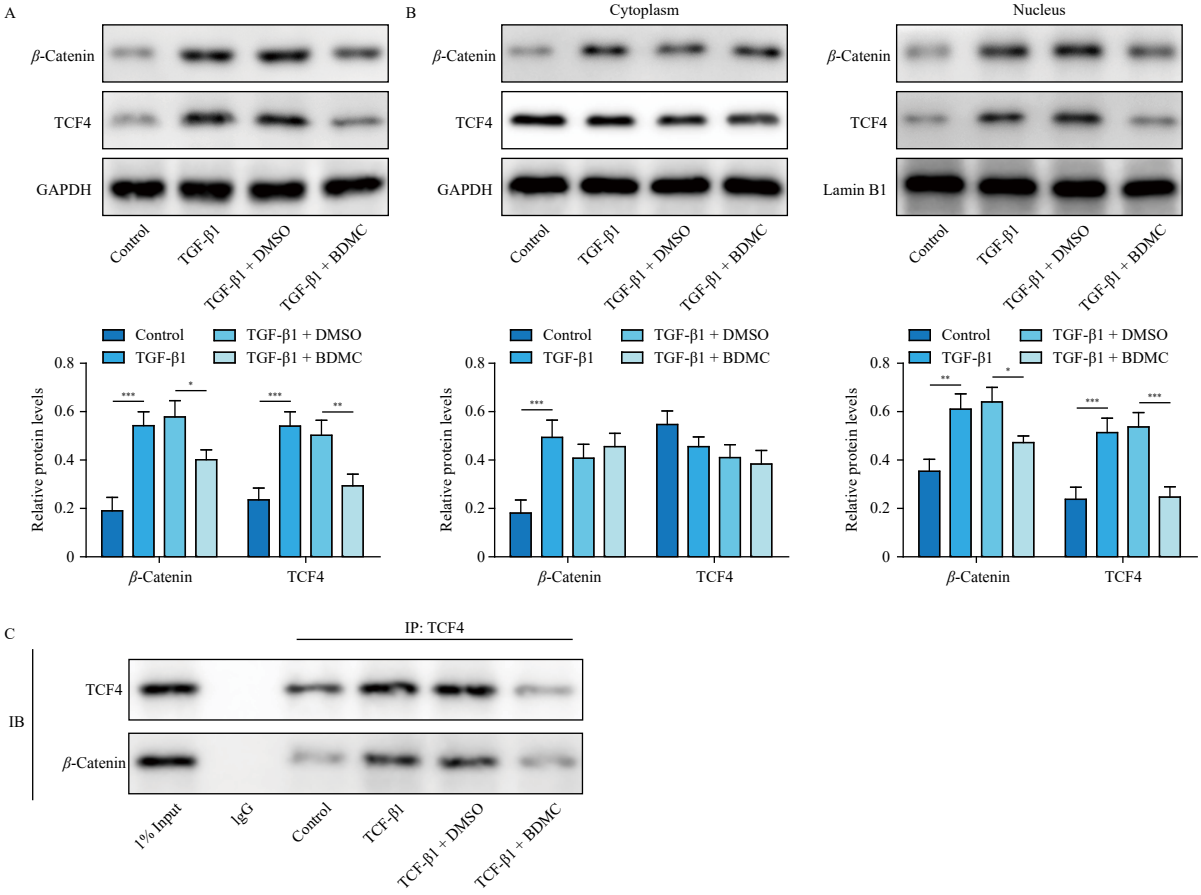

Fig. 5 BDMC prevented the formation of *β*-catenin/TCF4 complex. (A) The expressions of *β*-catenin and TCF4 in LX-2 cells were measured by western blot. (B) *β*-Catenin and TCF4 levels in cytoplasm or nucleus of LX-2 cells were assessed by western blot. (C) The impact of BDMC on *β*-catenin/TCF4 complex formation was explored by Co-IP in LX-2 cells. Data were expressed as mean ± SD. All our data were obtained from three independent experiments. $^{*}P < 0.05$, $^{**}P < 0.01$, $^{***}P < 0.001$.

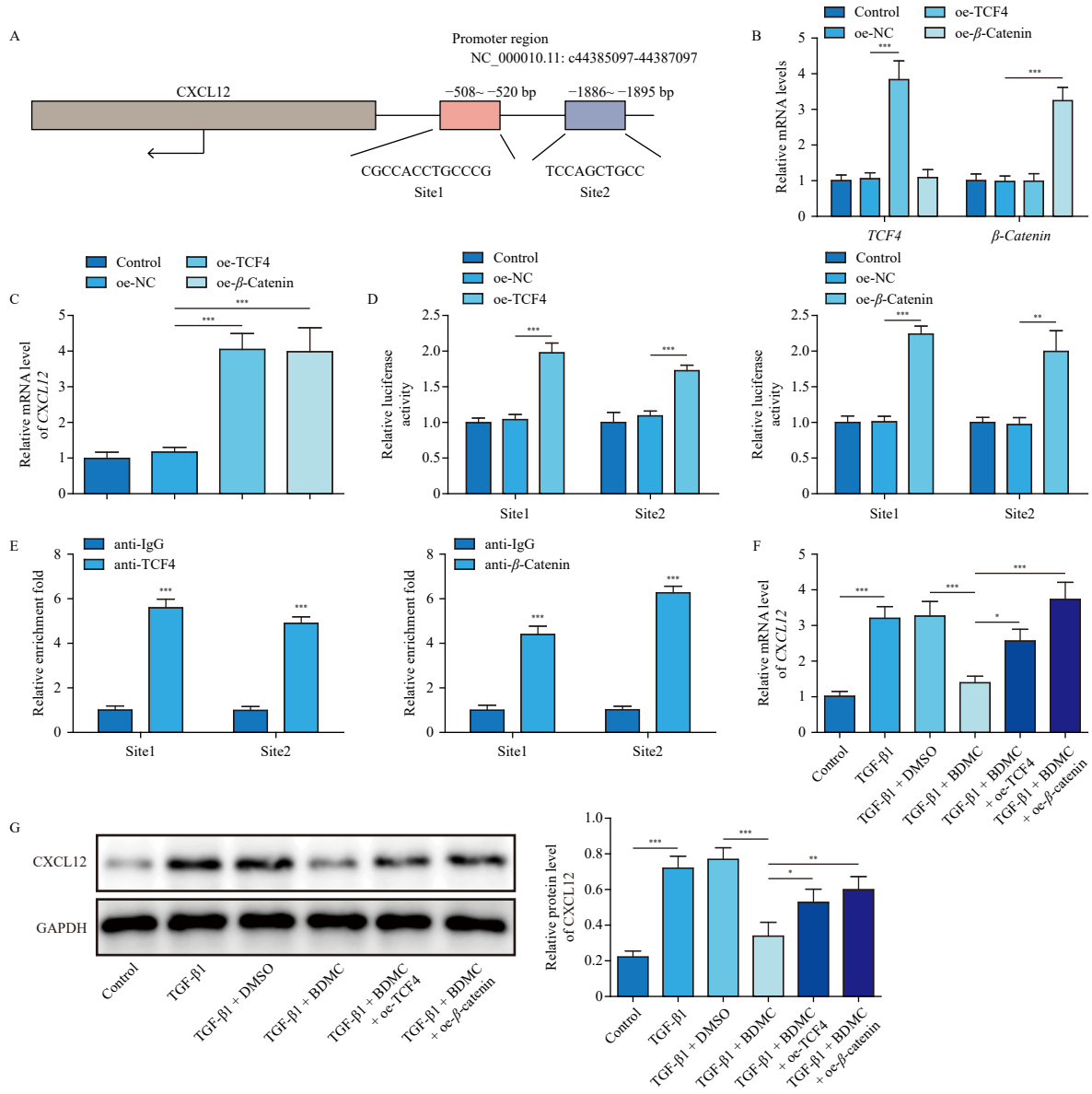

Fig. 6 BDMC inhibited CXCL12 transcription *via* suppressing β-catenin/TCF4. (A) The binding between CXCL12 and β-catenin/TCF4 complex was predicted by JASPAR software. LX-2 cells were exposed to pcDNA3.1-TCF4, pcDNA3.1 or pcDNA3.1-β-catenin. (B) The expressions of TCF4 and β-catenin were examined by RT-qPCR. (C) The level of CXCL12 was tested by RT-qPCR. (D) The luciferase activity in CXCL12 promoter was tested by luciferase assay. (E) The binding between TCF4/β-catenin and the promoter region of CXCL12 was detected by ChIP in LX-2 cells. LX-2 cells were exposed to TGF-β1, TGF-β1 + DMSO, TGF-β1 + BDMC, TGF-β1 + BDMCs + pcDNA3.1-TCF4 or TGF-β1 + BDMCs + pcDNA3.1-β-catenin. (F & G) The level of CXCL12 was examined by RT-qPCR and western blot. Data were expressed as mean ± SD. All data were obtained from three independent experiments. $^{*}P < 0.05$, $^{**}P < 0.01$, $^{***}P < 0.001$.

3.8. CXCL12 reversed the inhibitory effect of BDMC on liver fibrosis and HCC cell function mediated by M2-like macrophages

Neither recombinant CXCL12 nor AMD3100 demonstrated significant impact on LX-2 cell viability (Fig. 8A). BDMC significantly decreased α-SMA, collagen I, and fibronectin expression in LX-2 cells; this effect was partially reversed by CXCL12 upregulation but enhanced by AMD3100 (Fig. 8B–8C). Moreover, BDMC suppressed HCC cell viability, migration, proliferation, and invasion induced by PMA-differentiated THP-1 cells co-cultured with TGF-β1-induced LX-2 cells. This effect was reversed by recombinant CXCL12 but enhanced by AMD3100 (Fig. 8D–8G). BDMC elevdecreased N-cadherin levels in co-cultured HCC cells; this effect was inhibited by recombinant CXCL12, while AMD3100 amplified BDMC's effects (Fig. 8H). These findings demonstrate that BDMC attenuated liver fibrosis and PMA-differentiated THP-1 cells-mediated HCC cell function *via* CXCL12.

3.9. BDMC attenuated DEN-induced liver fibrosis progression to HCC via downregulating CXCL12

To investigate the role of BDMC and CXCL12 in the progression from liver fibrosis to HCC, an animal study was conducted (Fig. 9A). As shown in Fig. 9B, DEN significantly reduced rat body weight from the inflammation stage (week 6) through the fibrosis stage (week 12) to the HCC stage (week 20). This effect was reversed by BDMC but further enhanced by recombinant CXCL12. Similarly, serum levels of ALT, AST, HA, LN, P-III-NP, and IV-C were significantly elevated by DEN, which was mitigated by BDMC but further increased by recombinant CXCL12 from the inflammation stage (week 6) through the fibrosis stage (week 12) to the HCC stage (week 20) (Figs. 9C–9D). Additionally, CXCL12 partially reversed the BDMC-induced reduction in these factors (Figs. 9C–9D). In the DEN rat model, BDMC treatment decreased the expression of M2-type markers TGF-β1, IL-10 and Arg-1, while recombinant CXCL12 counteracted the effect of BDMC

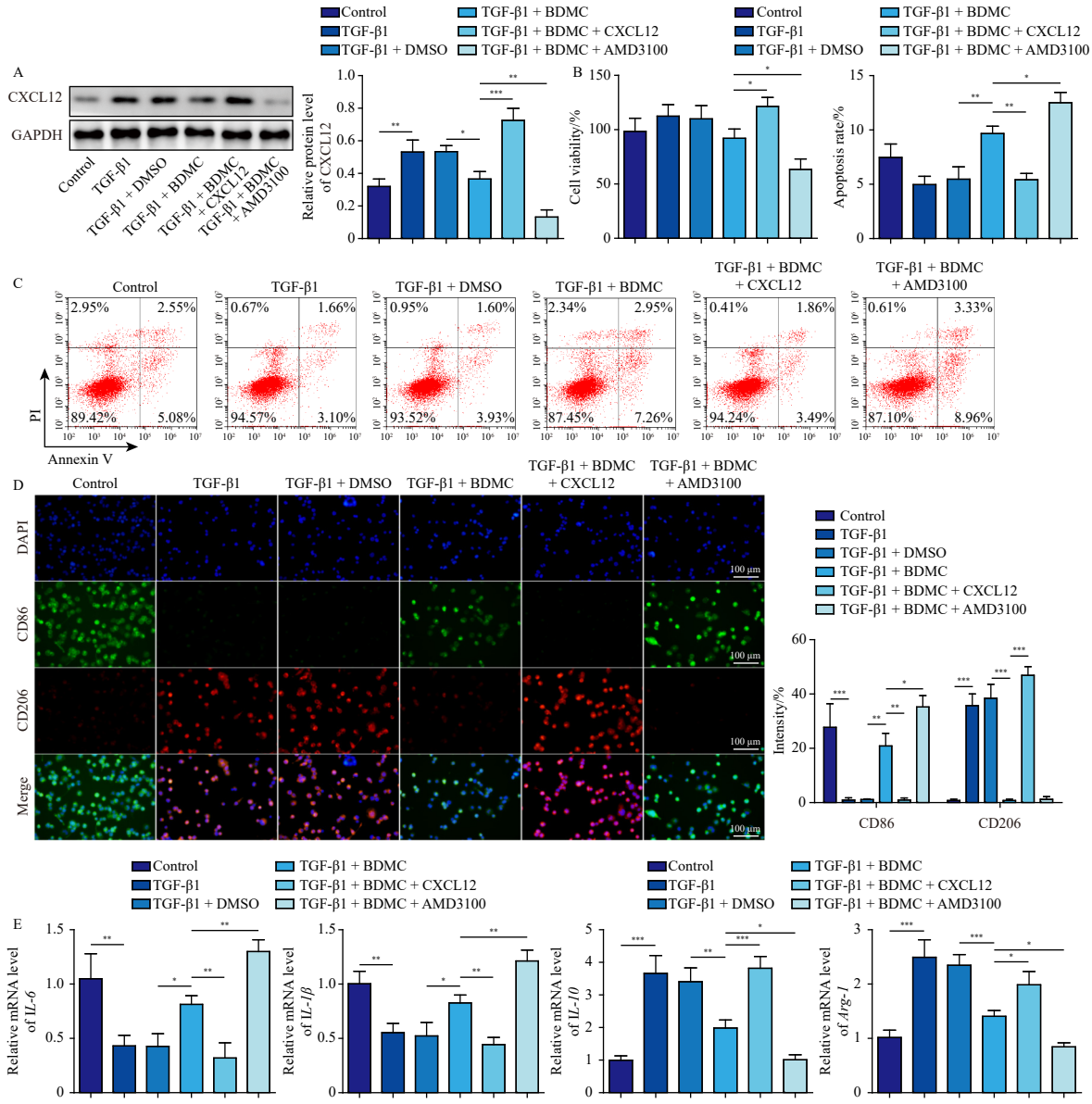

Fig. 7 CXCL12 reversed BDMC's inhibition of M2 polarization of macrophages caused by activated HSCs. LX-2 cells were exposed to TGF-β1, TGF-β1 + DMSO, TGF-β1 + BDMC, TGF-β1 + BDMC + recombinant CXCL12, TGF-β1 + BDMC + AMD3100 (5 nM). (A) The level of CXCL12 in LX-2 cells was tested by western blot. (B) The viability of LX-2 cells was tested by immunofluorescence staining. (C) The apoptosis of LX-2 cells was tested by flow cytometry. LX-2 cells with different treatment were then co-cultured th THP-1 cells. After that, THP-1 cells were collected. (D) The levels of CD86 and CD206 were detected by immunofluorescence staining. (E) The levels of IL-6, IL-1β, L-10 and Arg-1 in co-cultured THP-1 cells were measured by RT-qPCR. Data were expressed as mean ± SD. All data were obtained from three independent experiments. $^{*}P < 0.05$, $^{**}P < 0.01$, $^{***}P < 0.001$.

(Fig. 9E). DEN-induced elevation of liver/body weight ratio was significantly reduced by BDMC, an effect that was negated by recombinant CXCL12 (Fig. 9F). Moreover, DEN accelerated the progression of hepatic "inflammation-fibrosis-carcinoma transformation", and the liver of DEN group rats displayed distinct pathological features at various stages, including chronic inflammatory infiltrates (6th week), fibrosis and cirrhosis (12th week), and high or middle differentiation of HCC (20th week) (Figs. 9G–9H). These changes were significantly suppressed by BDMC but exacerbated by recombinant CXCL12 (Figs. 9G–9H). Recombinant CXCL12 reversed BDMC's inhibitory effect on hepatic "inflammation-fibrosis-carcinoma transformation" (Figs. 9G–9H). As illustrated in Fig. 9I,

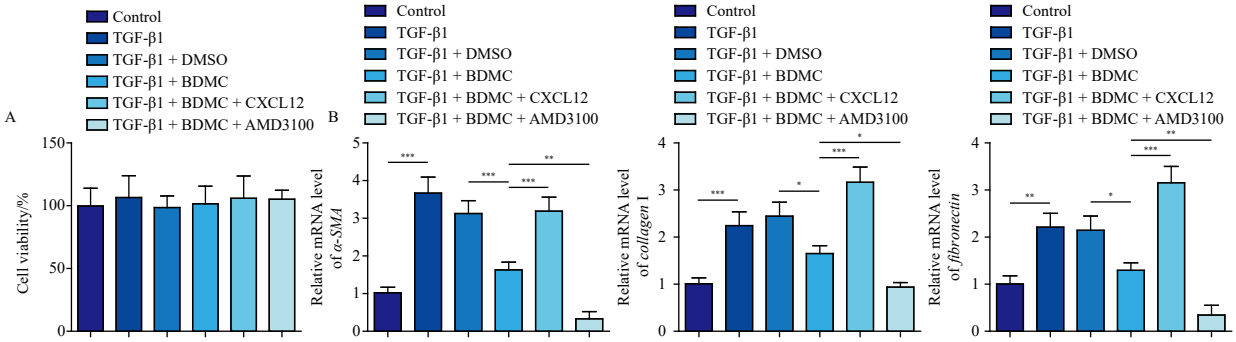

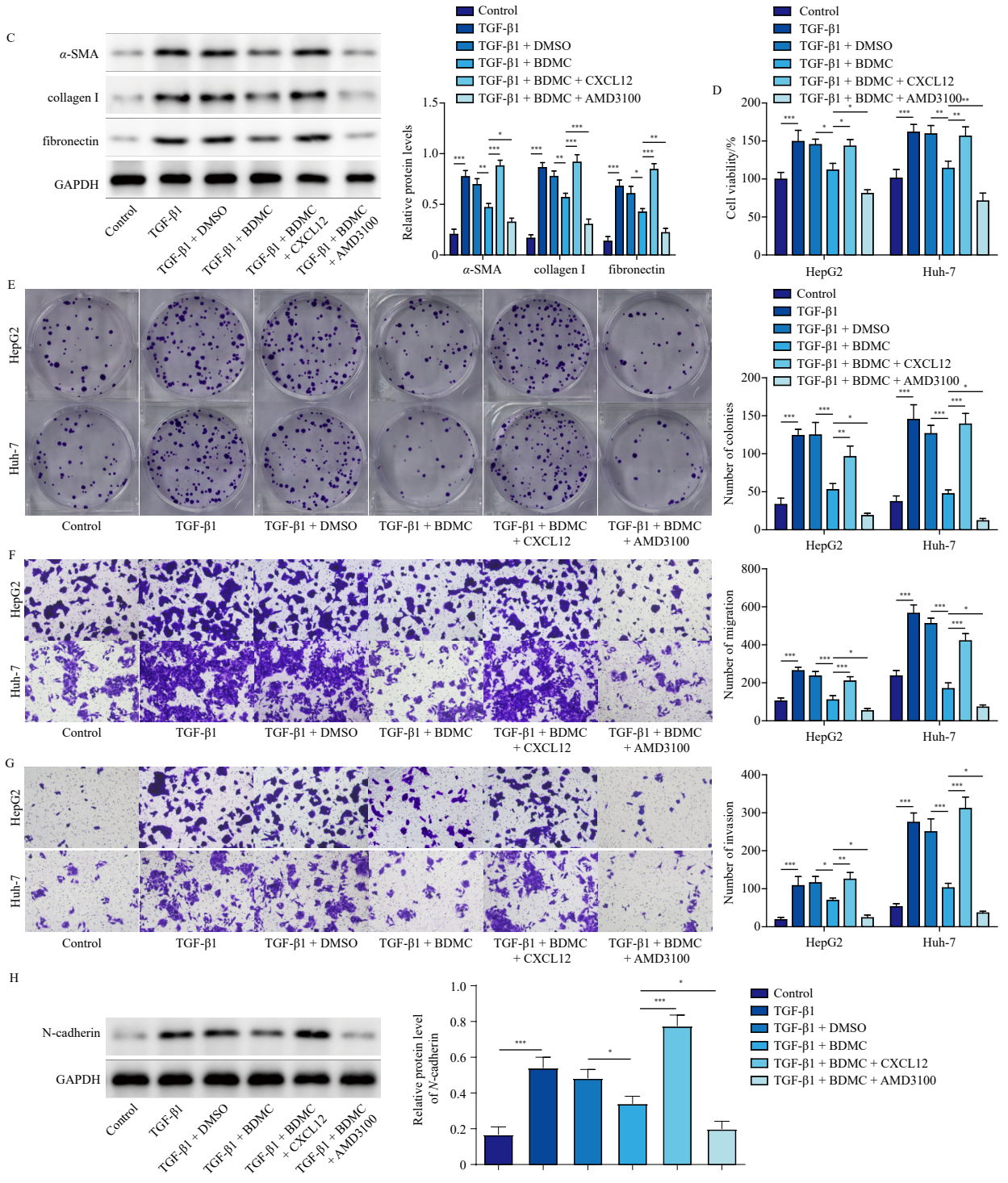

Fig. 8 CXCL12 reversed the inhibitory effect of BDMC on liver fibrosis and HCC cell function mediated by M2 macrophages. THP-1 cells were co-cultured with different treatment of LX-2 cells before being co-cultured with LX-2 cells and HCC cells separately, and then LX-2 cells and HCC cells were isolated for further analysis. (A) The viability of co-cultured LX-2 cells was assessed by MTT assay. (B & C) The levels of α-SMA, collagen I and fibronectin in co-cultured LX-2 cells were tested by RT-qPCR and western blot. (D–G) The viability, proliferation, migration and invasion of co-cultured HCC cells were tested by MTT, colony formation and transwell assay, respectively. (H) The levels of N-cadherin in co-cultured HCC cells were tested by western blot. Data were expressed as mean ± SD. All data were obtained from three independent experiments. $^{*}P < 0.05$, $^{**}P < 0.01$, $^{***}P < 0.001$.

the DEN group progressed from normal morphology to substantial structural alterations, including multiple white nodules and balloon-like structures on the liver surface (20th week). These effects were diminished by BDMC but amplified by recombinant CXCL12 (Fig. 9I). Furthermore, recombinant CXCL12 partially counteracted the BDMC-induced reduction of liver surface nodules (Fig. 9I). IHC staining revealed that BDMC significantly reduced the expressions of α-SMA, collagen I, CXCL12 and CD206 in DEN-induced rats, while CXCL12 demonstrated opposing effects (Fig. S1). Moreover, the inhibitory effect of BDMC was substantially diminished by recombinant CXCL12 (Fig. S1). Thus, BDMC mitigated DEN-induced liver fibrosis progression to HCC through CXCL12 inhibition.

4. Discussion

Chronic liver inflammation and the resulting cirrhosis microenvironment are established factors that promote the occur-

rence and development of HCC [37]. Therefore, preventing the progression of hepatic "inflammation-fibrosis-carcinoma transformation" is crucial for HCC prevention.

Macrophages constitute fundamental components of innate immunity and serve a crucial role in the tumor microenvironment. The dynamics of macrophage phenotypes are influenced by the duration and intensity of inflammation, fibrosis, and cancer [38]. Macrophage phenotypic alterations are also determined by the liver's microenvironment during hepatic injury [39]. Research suggests that M1 polarization may contribute to fibrosis-cirrhosis progression [40, 41]. Furthermore, M1 polarized cells derived from bone marrow macrophages can suppress liver fibrosis progres-

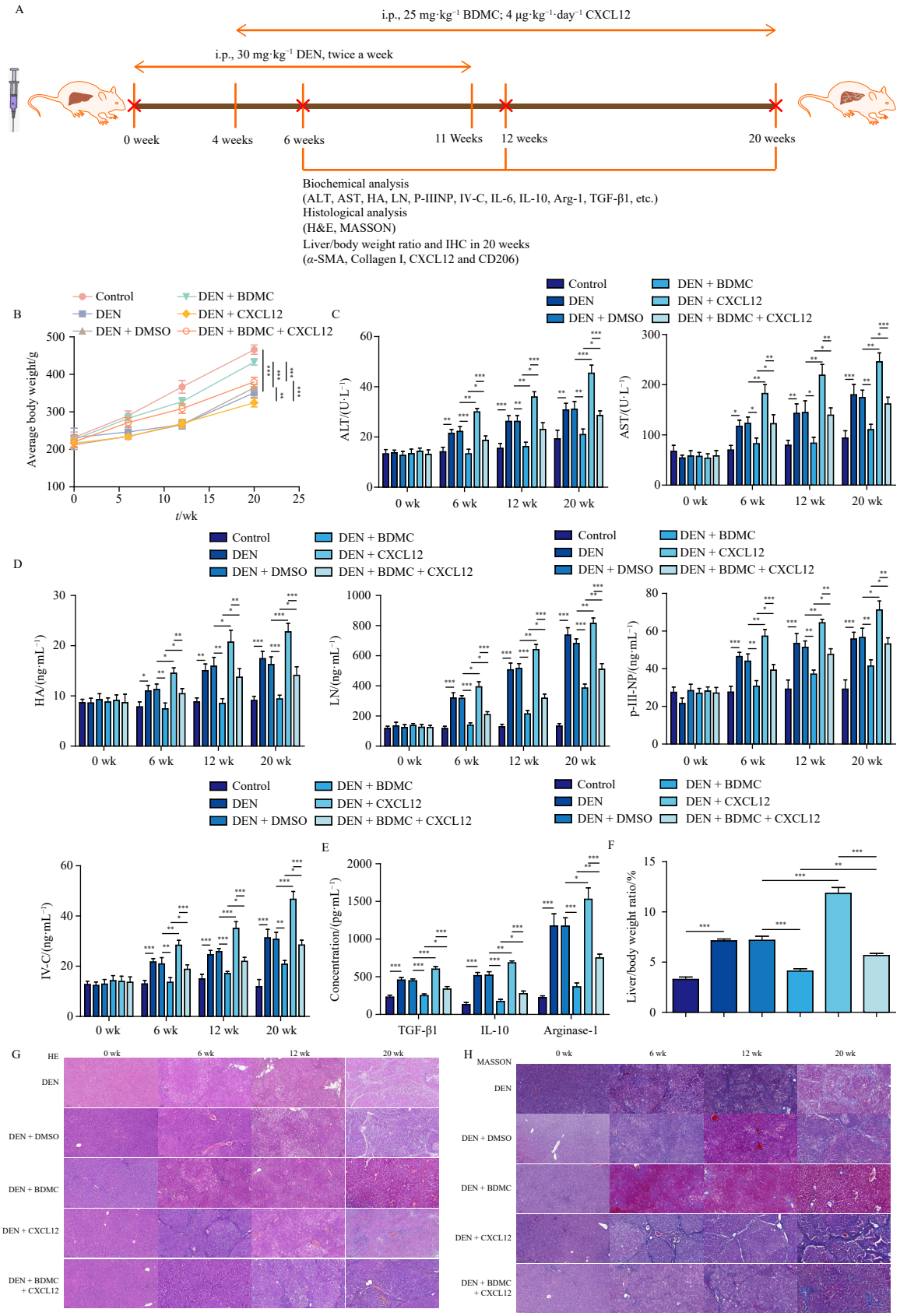

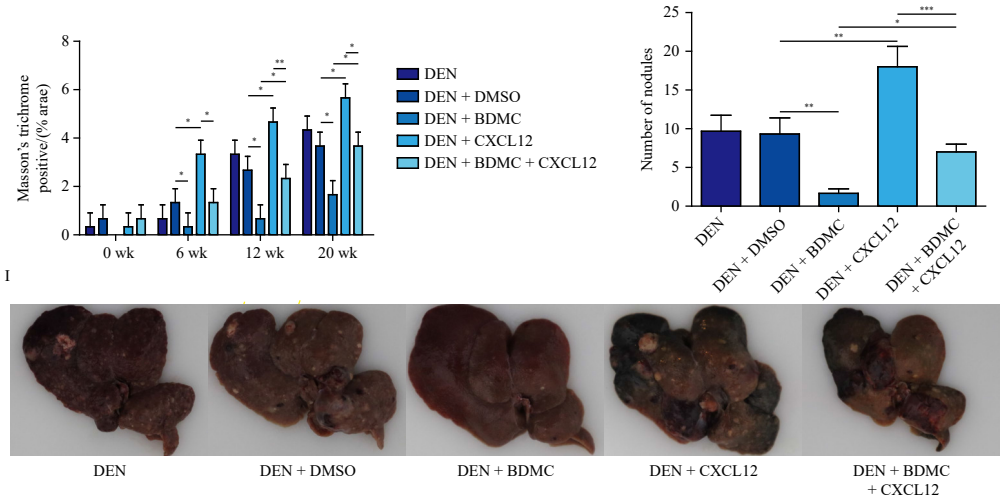

Fig. 9 BDMC attenuated DEN-induced liver fibrosis progression to HCC via downregulating CXCL12. (A) Animal experiments and sampling flowchart was presented. The DEN group was administrated 30 mg·kg^{-1} DEN (Sigma-Aldrich) twice a week for 11 weeks. BDMC was administered intraperitoneally at 25 mg·kg^{-1} every other day starting at week 4. Recombinant CXCL12 (4 μg·kg^{-1}·d^{-1}) was administered from week 4 through to week 20 to investigate its role in reversing the inhibitory effects of BDMC on liver fibrosis and HCC development. (B) The body weight was measured. (C) The contents of AST and ALT were assessed by biochemical kits. (D) The levels of HA, LN, P-III-NP and IV-C in serum of rats were tested by ELISA kits. (E) The levels of IL-10, Arg-1, and TGF-β1 were examined by ELISA kits. (F) The liver/body weight ratio in rats was calculated. (G & H) The histological changes in rat liver tissues were tested by H&E and Masson staining. (I) The images of liver tissue were presented. Data were expressed mean ± SD (n = 6).$^{*}P$ < 0.05, $^{**}P$ < 0.01, $^{***}P$ < 0.001. Original magnification: 100 × .

sion [42], indicating a strong correlation between macrophage polarization and liver fibrosis. HSC activation enhances M2 macrophage polarization, thereby promoting liver fibrosis and HCC development [43, 44]. Research has demonstrated that activated HSCs promoted M2 polarization of macrophages, subsequently inducing HCC cell invasion [35, 45]. Consequently, understanding the regulatory mechanisms of macrophage polarization holds significant importance for developing novel therapeutic strategies for LFAHCC. Aligned with previous research, our findings demonstrated that HSCs-mediated liver fibrosis and enriched M2 macrophages were observable in HCC tissues. The selected time points for monitoring liver inflammation (week 6), fibrosis (week 12), and HCC (week 20) were based on previous studies using the DEN rat model [4]. Our results corroborated these earlier findings. Additionally, HSCs-mediated liver fibrosis and enriched M2 macrophages were detected in DEN-treated rat liver tissues, while TGF-β1-induced LX-2 cells promoted macrophage M2 polarization *in vitro*. These findings support the conclusion that activated HSCs promoted liver fibrosis and macrophage M2 polarization, which were associated with HCC.

BDMC exerts anti-tumor activities in various human malignant tumors [19, 46]. As evidence, BDMC treatment markedly inhibited the proliferation of HCC cells [22]. In addition, BDMC treatment could relieve liver fibrosis by inducing HSC apoptosis [21]. However, BDMC's role in preventing hepatic "inflammation-fibrosis-carcinoma transformation" remains unclear. Our current results revealed that BDMC inhibited fibrosis and HCC cell proliferation and migration by reducing HSCs-induced M2 macrophage polarization. These findings represent the first identification of BDMC's inhibitory function in the fibrosis-cirrhosis-cancer axis. While BDMC administration at four weeks post-DEN-induced liver inflammation may appear early, before cirrhosis development, chronic inflammation represents a well-established precursor to liver fibrosis and HCC. BDMC exhibits significant anti-inflammatory properties, particularly in hepatitis, through inhibition of the TGF-β and NF-κB pathways, which are fundamental to liver injury [20]. Early intervention during the inflammation stage is essential, as it may prevent progression to fibrosis and carcinoma.

Research has extensively documented BDMC's regulation of multiple signaling pathways in tumor progression. Liao CL *et al.* demonstrated that BDMC inactivates the NF-κB signaling pathway in cervical cancer [47]. Furthermore, BDMC inactivates Akt signaling in osteosarcoma cells [48]. The chemokine CXCL12 facilitates macrophage polarization, HSC activation, and HCC progression. Previous research showed that miR-155 inhibits HSC activation through the CXCL12/CXCR4 axis [49]. Significantly, activated HSCs induced M2 polarization of macrophages by producing CXCL2, potentially relating to LFAHCC progression [12]. The current study revealed markedly elevated CXCL12 levels in activated HSCs and the DEN-induced rat model during LFAHCC progression, with this elevation neutralized by BDMC treatment. Additionally, recombinant CXCL12 addition reversed BDMC's inhibitory effect on liver fibrosis and HCC cell function mediated by M2 macrophages. These results indicate that BDMC inhibited liver fibrosis and HCC induced by M2-like macrophages through CXCL2 suppression.

The Wnt/β-catenin pathway serves as a crucial signaling pathway in M2 macrophage polarization-mediated tumor progression [50, 51]. Previous research has demonstrated that BDMC treatment could inactivate the Wnt/β-catenin signaling pathway [52]. In the present study, findings indicate that BDMC inhibits β-catenin nuclear translocation and the formation of the β-catenin/TCF4 complex, suggesting that the β-catenin/TCF4 complex may be involved in BDMC-mediated inhibition of macrophage M2 polarization. The β-catenin/TCF4 complex promotes cancer progression, and its formation facilitates the transcriptional expression of downstream target genes [51, 53]. CXCL12 functions as a potent chemotactic factor that recruits macrophages in colitis-associated colorectal cancer [15]. The relationship between BDMC regulation of CXCL12 through β-catenin/TCF4 remained unexplored. The results demonstrate that BDMC reduces β-catenin/TCF4 complex formation, thereby inhibiting β-catenin and TCF4-modulated transcriptional activation of CXCL12.

5. Conclusion

In conclusion, this study demonstrates a novel application of BDMC in treating liver inflammation, fibrosis, and HCC. The findings provide evidence that BDMC intervenes early during the inflammatory phase of liver disease, preventing progression to fibrosis and cancer by targeting macrophage M2 polarization through reduced β-catenin/TCF4-mediated CXCL12 transcription (Fig. 10). This research highlights BDMC's potential as an effective therapeutic option, presenting new possibilities for man-

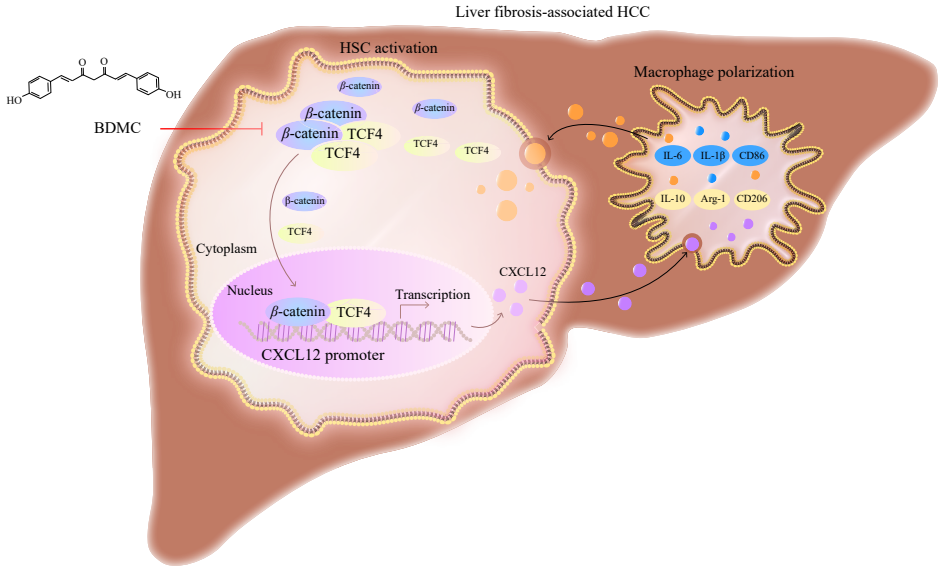

Fig. 10 The schematic illustration of this study. BDMC repressed the progression of liver fibrosis towards HCC *via* inhibiting M2 macrophage polarization by decreasing *β*-catenin/TCF4-mediated CXCL12 transcription.

aging and preventing chronic liver diseases, including HCC. The significance of these findings lies in the early-stage intervention and the mechanisms through which BDMC exerts its protective effects, establishing it as a promising candidate for clinical translation. Several limitations exist in this research. The downstream target of CXCL12 in regulating M2 macrophage polarization during liver fibrosis progression towards HCC remains uninvestigated. Future studies will address this deficiency to strengthen the research conclusions. Additionally, the study lacked a positive control. This limitation warrants consideration when interpreting the results. Future research incorporating a positive control group will enhance the findings and provide more robust treatment effect comparisons.

Funding

This work was supported by the National Natural Science Foundation of China (No. 81904182), the Training Program for Excellent Young Innovators of Changsha (No. kq2209020), the Excellent Youth Project of Hunan University of Chinese Medicine (No. 2022XJB006), and the Excellent Youth Project of Natural Science Foundation of Heilongjiang Province (No. YQ2022H015).

Declaration of competing interest

These authors have no conflict of interest to declare.

References

1 Sung H, Ferlay F, Siegel RL, et al. Global Cancer Statistics 2020: GLOBOCAN estimates of incidence and mortality worldwide for 36 cancers in 185 countries. *CA Cancer J Clin*. 2021;71:209-249. https://doi.org/10.3322/caac.21660.
2 Chidambaranathan-Reghupaty S, Fisher PB, Sarkar D. Hepatocellular carcinoma (HCC): epidemiology, etiology and molecular classification. *Adv Cancer Res*. 2021;149:1-61. https://doi.org/10.1016/bs.acr.2020.10.001.
3 Korbecki J, Simińska D, Gąssowska-Dobrowolska M, et al. Chronic and cycling hypoxia: drivers of cancer chronic inflammation through HIF-1 and NF-κB activation. *Int J Mol Sci*. 2021;22(9):10701. https://doi.org/10.3390/ijms221910701.
4 Ding YF, Wu ZH, Wei YJ, et al. Hepatic inflammation-fibrosis-cancer axis in the rat hepatocellular carcinoma induced by diethylnitrosamine. *J Cancer Res Clin Oncol*. 2017;143(5):821-834. https://doi.org/10.1007/s00432-017-2364-z.
5 Ringelhan M, Pfister D, O'Connor T, et al. The immunology of hepatocellular carcinoma. *Nat Immunol*. 2018;19(3):222-232. https://doi.org/10.1038/s41590-018-0044-z.
6 Myojin Y, Hikita H, Sugiyama M, et al. Hepatic stellate cells in hepatocellular carcinoma promote tumor growth *via* growth differentiation factor 15 production. *Gastroenterology*. 2021;160(5):1741-1754.e16. https://doi.org/10.1053/j.gastro.2020.12.015.
7 Zhang R, Yao RR, Li JH, et al. Activated hepatic stellate cells secrete periostin to induce stem cell-like phenotype of residual hepatocellular carcinoma cells after heat treatment. *Sci Rep*. 2017;7:2164. https://doi.org/10.1038/s41598-017-01177-6.
8 Zheng X, Jiang Q, Han M, et al. FBXO38 regulates macrophage polarization to control the development of cancer and colitis. *Cell Mol Immunol*. 2023;20(12):1367-1378. https://doi.org/10.1038/s41423-023-01081-2.
9 Vitale I, Manic G, Coussens LM, et al. Macrophages and metabolism in the tumor microenvironment. *Cell Metab*. 2019;30(1):36-50. https://doi.org/10.1016/j.cmet.2019.06.001.
10 Yin L, Shi C, Zhang Z, et al. Formosanin C attenuates lipopolysaccharide-induced inflammation through nuclear factor-κB inhibition in macrophages. *Korean J Physiol Pharmacol*. 2021;25(5):395-401. https://doi.org/10.4196/kjpp.2021.25.5.395.
11 Cao D, Naiyila X, Li J, et al. Potential strategies to improve the effectiveness of drug therapy by changing factors related to tumor microenvironment. *Front Cell Dev Biol*. 2021;9:705280. https://doi.org/10.3389/fcell.2021.705280.
12 Matsuda M, Seki E. Hepatic stellate cell-macrophage crosstalk in liver fibrosis and carcinogenesis. *Semin Liver Dis*. 2020;40(3):307-320. https://doi.org/10.1055/s-0040-1708876.
13 Hao X, Zheng Z, Liu H, et al. Inhibition of APOC1 promotes the transformation of M2 into M1 macrophages *via* the ferroptosis pathway and enhances anti-PD1 immunotherapy in hepatocellular carcinoma based on single-cell RNA sequencing. *Redox Biol*. 2022;56:102463. https://doi.org/10.1016/j.redox.2022.102463.
14 Casari M, Siegl D, Deppermann C, et al. Macrophages and platelets in liver fibrosis and hepatocellular carcinoma. *Front Immunol*. 2023;14:1277808. https://doi.org/10.3389/fimmu.2023.1277808.
15 Wu S, Yuan W, Luo W, et al. miR-126 downregulates CXCL12 expression in intestinal epithelial cells to suppress the recruitment and function of macrophages and tumorigenesis in a murine model of colitis-associated colorectal cancer. *Mol Oncol*. 2022;16(18):3465-3489. https://doi.org/10.1002/1878-0261.13218.
16 Chiraunyanann T, Changsri K, Sretapunya W, et al. CXCL12 G801A polymorphism is associated with significant liver fibrosis in HIV-infected Thais: a cross-sectional study. *Asian Pac J Allergy Immunol*. 2019;37(3):162-170. https://doi.org/10.12932/AP-160917-0162.
17 Chalin A, Lefevre B, Devisme C, et al. Circulating levels of CXCL11 and CXCL12 are biomarkers of cirrhosis in patients with chronic hepatitis C infection. *Cytokine*. 2019;117:72-78. https://doi.org/10.1016/j.cyto.2019.02.006.
18 Yang R, Shen H, Wang M, et al. Expression of SDF-1/CXCR4 and related inflammatory factors in sodium fluoride-treated hepatocytes. *PLoS One*. 2024;19(1):e0302530. https://doi.org/10.1371/journal.pone.0302530.
19 Miklasova N, Herich P, Davila-Becerril JC, et al. Evaluation of antiproliferative palladium (II) complexes of synthetic bisdemethoxycurcumin towards *in vitro* cytotoxicity and molecular docking on DNA sequence. *Molecules*. 2021;26(4):1048. https://doi.org/10.3390/molecules26144369.
20 Gan Y, Zheng S, Zhao J, et al. Protein network module-based identification of key pharmacological pathways of *Curcuma phaeocaulis* Val. acting on hepatitis. *J Ethnopharmacol*. 2018;221:10-19. https://doi.org/10.1016/j.jep.2018.03.004.
21 Lee PJ, Woo SJ, Jee JG, et al. Bisdemethoxycurcumin induces apoptosis in activated hepatic stellate cells *via* cannabinoid receptor 2. *Molecules*. 2015;20(7):1277-1292. https://doi.org/10.3390/molecules20011277.
22 Qiu C, Liu K, Zhang S, et al. Bisdemethoxycurcumin inhibits hepatocellular carcinoma proliferation through Akt inactivation *via* CYLD-mediated

deubiquitination. *Drug Des Devel Ther*. 2020;14:993-1001. https://doi.org/10.2147/DDDT.S231814.
23 Katoh M. Multi-layered prevention and treatment of chronic inflammation, organ fibrosis and cancer associated with canonical WNT/*β*-catenin signaling activation. *Int J Mol Med*. 2018;42(2):713-725. https://doi.org/10.3892/ijmm.2018.3689.
24 Akcora BO, Storm G, Bansal R. Inhibition of canonical WNT signaling pathway by *β*-catenin/CBP inhibitor ICG-001 ameliorates liver fibrosis *in vivo* through suppression of stromal CXCL12. *Biochim Biophys Acta Mol Basis Dis*. 2018;1864(3):804-818. https://doi.org/10.1016/j.bbadis.2017.12.001.
25 Vilchez V, Turcios L, Marti F, et al. Targeting Wnt/*β*-catenin pathway in hepatocellular carcinoma treatment. *World J Gastroenterol*. 2016;22(2):823-832. https://doi.org/10.3748/wjg.v22.i2.823.
26 Liu YL, Yang HP, Zhou XD, et al. The hypomethylation agent bisdemethoxycurcumin acts on the WIF-1 promoter, inhibits the canonical Wnt pathway and induces apoptosis in human non-small-cell lung cancer. *Curr Cancer Drug Targets*. 2011;11(9):1098-1110. https://doi.org/10.2174/156800911798073041.
27 Tang Y, Jiang M, Chen A, et al. Porcupine inhibitor LGK974 inhibits Wnt/β-catenin signaling and modifies tumor-associated macrophages resulting in inhibition of the malignant behaviors of non-small cell lung cancer cells. *Mol Med Rep*. 2021;24(4):710. https://doi.org/10.3892/mmr.2021.12189.
28 Tewari D, Bawari S, Sharma S, et al. Targeting the crosstalk between canonical Wnt/*β*-catenin and inflammatory signaling cascades: a novel strategy for cancer prevention and therapy. *Pharmacol Ther*. 2021;227:107876. https://doi.org/10.1016/j.pharmthera.2021.107876.
29 Blosser SL, Sawyer N, Maksimovic I, et al. Covalent and noncovalent targeting of the Tcf4/*β*-catenin strand interface with *β*-hairpin mimics. *ACS Chem Biol*. 2021;16(8):1518-1525. https://doi.org/10.1021/acschembio.1c00389.
30 García de Herreros A, Dunach M. Intracellular signals activated by canonical Wnt ligands independent of GSK3 inhibition and *β*-catenin stabilization. *Cells*. 2019;8(10):1148. https://doi.org/10.3390/cells8101148.
31 Kim H, Jung J, Lee M, et al. *Curcuma longa* L. extract exhibits anti-inflammatory and cytoprotective functions in the articular cartilage of monoiodoacetate-injected rats. *Food Nutr Res*. 2024;68:10402 https://doi.org/10.29219/fnr.v68.10402.
32 Ding YF, Peng ZX, Ding L, et al. Baishouwu extract suppresses the development of hepatocellular carcinoma *via* TLR4/MyD88/NF-*κ*B pathway. *Front Pharmacol*. 2019;10:389. https://doi.org/10.3389/fphar.2019.00389.
33 Li X, Huai Q, Zhu C, et al. GDF15 ameliorates liver fibrosis by metabolic reprogramming of macrophages to acquire anti-inflammatory properties. *Cell Mol Gastroenterol Hepatol*. 2023;16:711-734. https://doi.org/10.1016/j.jcmgh.2023.07.009.
34 Colapietro A, Yang P, Rossetti A, et al. The botanical drug PBI-05204, a supercritical CO_2 extract of *Nerium oleander*, inhibits growth of human glioblastoma, reduces Akt/mTOR activities, and modulates GSC cell-renewal properties. *Front Pharmacol*. 2020;11:552428. https://doi.org/10.3389/fphar.2020.552428.
35 Xue J, Xiao T, Wei S, et al. miR-21-regulated M2 polarization of macrophage is involved in arsenicosis-induced hepatic fibrosis through the activation of hepatic stellate cells. *J Cell Physiol*. 2021;236:6025-6041. https://doi.org/10.1002/jcp.30288.
36 Vallée A, Lecarpentier Y, Vallée JN, et al. Curcumin: a therapeutic strategy in cancers by inhibiting the canonical WNT/β-catenin pathway. *J Exp Clin Cancer Res*. 2019;38:323. https://doi.org/10.1186/s13046-019-1320-y.
37 Yang YM, Kim SY, Seki E. Inflammation and liver cancer: molecular mechanisms and therapeutic targets. *Semin Liver Dis*. 2019;39:26-42. https://doi.org/10.1055/s-0038-1676806.
38 Tacke F. Targeting hepatic macrophages to treat liver diseases. *J Hepatol*. 2017;66:1300-1312. https://doi.org/10.1016/j.jhep.2017.02.026.
39 Sica A, Invernizzi P, Mantovani A, et al. Macrophage plasticity and polarization in liver homeostasis and pathology. *Hepatology*. 2014;59:2034-2042. https://doi.org/10.1002/hep.26754.
40 Caligiuri A, Gentilini A, Pastore M, et al. Cellular and molecular mechanisms underlying liver fibrosis regression. *Cells*. 2021;10:231. https://doi.org/10.3390/cells10102759.
41 Martínez-Esparza M, Tristán-Manzano M, Ruiz-Alcaraz AJ, et al. Inflammatory status in human hepatic cirrhosis. *World J Gastroenterol*. 2015;21:11522-11541. https://doi.org/10.3748/wjg.v21.i41.11522.
42 Ma PF, Gao CC, Yi J, et al. Cytotherapy with M1-polarized macrophages ameliorates liver fibrosis by modulating immune microenvironment in mice. *J Hepatol*. 2017;67:770-779. https://doi.org/10.1016/j.jhep.2017.05.022.
43 Pivovarova-Ramich O, Loske J, Hornemann S, et al. Hepatic WISP1/CCN4 associates with markers of liver fibrosis in severe obesity. *Cells*. 2021;10:1048. https://doi.org/10.3390/cells10051048.
44 Yan Q, Pan L, Qi S, et al. RNF2 mediates hepatic stellate cells activation by regulating ERK/p38 signaling pathway in LX-2 cells. *Front Cell Dev Biol*. 2021;9:634902. https://doi.org/10.3389/fcell.2021.634902.
45 Robert S, Gicquel T, Bodin A, et al. Influence of inflammasome pathway activation in macrophages on the matrix metalloproteinase expression of human hepatic stellate cells. *Int Immunopharmacol*. 2019;72:12-20. https://doi.org/10.1016/j.intimp.2019.03.060.
46 Guo F, Xia T, Xiao P, et al. A supramolecular complex of hydrazide-pillar[5]arene and bisdemethoxycurcumin with potential anti-cancer activity. *Bioorg Chem*. 2021;110:104764. https://doi.org/10.1016/j.bioorg.2021.104764.
47 Liao CL, Chu YL, Lin HY, et al. Bisdemethoxycurcumin suppresses migration and invasion of human cervical cancer HeLa cells *via* inhibition of NF-*κ*B, MMP-2 and -9 pathways. *Anticancer Res*. 2018;38:3989-3997. https://doi.org/10.21873/anticanres.12686.
48 Huang C, Lu HF, Chen YH, et al. Curcumin, demethoxycurcumin, and bisdemethoxycurcumin induced caspase-dependent and -independent apoptosis *via* Smad or Akt signaling pathways in HOS cells. *BMC Complement Med Ther*. 2020;20:68. https://doi.org/10.1186/s12906-020-2857-1.
49 Zhang C, Hang Y, Tang W, et al. Dually active polycation/miRNA nanoparticles for the treatment of fibrosis in alcohol-associated liver disease. *Pharmaceutics*. 2022;14:425. https://doi.org/10.3390/pharmaceutics14030669.
50 Akasu M, Shimada S, Kabashima A, et al. Intrinsic activation of *β*-catenin signaling by CRISPR/Cas9-mediated exon skipping contributes to immune evasion in hepatocellular carcinoma. *Sci Rep*. 2021;11:16732. https://doi.org/10.1038/s41598-021-96167-0.
51 Low JL, Du W, Gocha T, et al. Molecular docking-aided identification of small molecule inhibitors targeting *β*-catenin-TCF4 interaction. *iScience*. 2021;24:102544. https://doi.org/10.1016/j.isci.2021.102544.
52 Joshi P, Joshi S, Semwal D, et al. Curcumin: an insight into molecular pathways involved in anticancer activity. *Mini Rev Med Chem*. 2021;21:2420-2457. https://doi.org/10.2174/1389557521666210122153823.
53 Sun J, Ma Q, Li B, et al. RPN2 is targeted by miR-181c and mediates glioma progression and temozolomide sensitivity *via* the Wnt/*β*-catenin signaling pathway. *Cell Death Dis*. 2020;11:890. https://doi.org/10.1038/s41419-020-03113-5.